PROCESSING AND CHARACTERIZATION OF NANO-ENGINEERED THIN FILMS

A Dissertation by

Mauricio E. Guzman

Master of Science, Wichita State University, USA, 2010

Bachelor of Science, Universidad Tecnologica del Centro, Venezuela, 2002

Submitted to the Department of Mechanical Engineering
and the faculty of the Graduate School of
Wichita State University
in partial fulfillment of
the requirements for the degree of
Doctor of Philosophy

August 2013

PROCESSING AND CHARACTERIZATION OF NANO-ENGINEERED THIN FILMS

The following faculty members have examined the final copy of this dissertation for form and content, and recommend that it be accepted in partial fulfillment of the requirement for the degree of Doctor of Philosophy, with a major in Mechanical Engineering.

_____
Bob Minaie, Committee Chair

_____
Brian Driessen, Committee Member

_____
Hamid Lankarani, Committee Member

_____
Krishna Krishna, Committee Member

_____
T.S. Ravigururajan, Committee Member

Accepted for the College of Engineering

_____
Vishwanath Prasad, Interim Dean

Accepted for the Graduate School

_____
Abu Masud, Interim Dean

DEDICATION

To God, my parents, my wife, my sisters,
and my dear friends

ACKNOWLEDGEMENTS

I would like to express the deepest appreciation to my advisor, Professor Bob Minaie, for giving me the opportunity to perform this work. Without his support, guidance, encouragement, and persistent help this dissertation would not have been possible. I would also like to extend my gratitude to Professor Brian Driessen, Professor Hamid Lankarani, Professor Krishna Krishna, and Professor T.S. Ravigururajan for serving on my dissertation committee.

I would like to thank Dr. Alejandro Rodriguez, who introduced me to the fascinating and complex world of composite materials and nanotechnology, and whose passion for research had lasting effect. I thank my colleagues in Professor Minaie's group, Chee Sern Lim, Ronald Joven, and Mohammad Amdadul Islam for their unconditional friendship and academic support. Their helpful comments and suggestions made this work more interesting and enjoyable.

To my wife, Satomi, I express the greatest appreciation. Her enthusiasm, patience, and unconditional support motivate me to reach my goals and objectives and make them possible.

ABSTRACT

Nanoparticle-based thin films are an emerging type of material with extraordinary electrical, mechanical, and physical properties. Because of their exceptional characteristics, these thin films can serve as reinforcement or conductive/semi-conductive sheets in composite and electronic systems. While most thin films comprise a structure of random nanoparticle network, the ability to produce high quality films depends on how to minimize inter-filler junction effects between filaments. This study presents a novel processing technique to fabricate thin films composed of functionalized carbon nanofibers (CNFs). The two-step process combines solution filtering and mechanical compression through a rolling process to form dense CNF thin films of uniform thickness. Electron micrographs show a remarkable change in surface morphology for all rolled films; the film morphology becomes more uniform and compact due to nanofiber displacement with mechanical compression. Test results show that tensile strength and electrical conductivity of surfactant-treated CNF films are inferior to those of oxidized CNF films. Based on these findings, it is suggested that surfactant significantly hinders the interaction between particles. Regarding the rolling effect on the oxidized CNF films, results show that strength and conductivity of rolled films improve by 400% with respect to the non-rolled films. By not having surfactant, it appears that the oxidized nanofibers can participate in higher intermolecular interactions and form an interlocking mechanism when forced into close proximity. Upon fracture, electron micrographs reveal significant pull-out and alignment of nanofibers for surfactant-treated CNF films as a result of particle slippage, while nanofiber fragmentation is identified for oxidized CNF films, suggesting higher fiber-fiber interaction within the dense entangled network. Hence, the methodology presented herein is an effective route to reduce inter-filler junction between nanofibers and to produce thin films with superior properties.

TABLE OF CONTENTS

LIST OF TABLES

LIST OF FIGURES

LIST OF FIGURES (continued)

x

LIST OF FIGURES (continued)

LIST OF ABBREVIATIONS/NOMENCLATURE

AC	Alternating Current
AR-CNF	As-received Carbon Nanofiber
ASTM	American Society for Testing Materials
CNF(s)	Carbon Nanofiber(s)
CNT(s)	Carbon Nanotube(s)
CVD	Chemical Vapor Deposition
DC	Direct Current
EDS	Energy-dispersive X-ray Spectroscopy
FTIR	Fourier-transform Infrared Spectrometry
IR	Infrared
MWCNT(s)	Multi-walled Carbon Nanotube(s)
OCNF(s)	Oxidized Carbon Nanofiber(s)
SEM	Scanning Electron Microscope
SWCNT(s)	Single-walled Carbon Nanotube(s)
TGA	Thermo-gravimetric Analyzer
VAC	Vacuum
VGCNF	Vapor-grown Carbon Nanofiber

LIST OF SYMBOLS

Å	Angstrom
Ar	Argon
CO	Carbon Monoxide
θ	Chiral Angle
$\vec{C}_h$	Chiral Vector
Cu	Copper
°	Degree
F/g	Farad/gram
GPa	Gigapascal
Δ	Heat
He	Helium
H	Hydrogen
Fe	Iron
LiCl	Lithium Chloride
MPa	Megapascal
μ	Micron
Mo	Molydenum
Ni	Nickel
$\Omega \cdot m$	Ohm.meter
O	Oxygen
$\delta^{\pm}$	Partial Charge
Pd	Palladium

LIST OF SYMBOLS (continued)

ppm   Part per million

π Pi

RPM   Revolutions per minute

Rh   Rhodium

V   Volt

wt%   Weight percent

Y   Yttrium

CHAPTER 1

INTRODUCTION

1.1.   Motivation and Scope

In Material Science and Engineering, the field of Carbon Science has evolved rapidly in the past few decades. Nanoparticles of zero, one, two, and three dimensions–fullerene, carbon nanotube/nanofiber, graphene, and diamond–have received considerable scientific and technical interest due to their outstanding material properties, not found in bulk materials. Carbon nanofiber, a carbon allotrope with an exceptional one-dimensional fiber-like structure, possesses a unique combination of mechanical, thermal, electrical, and physical properties. Recent reports estimate the tensile strength and elastic modulus of a single carbon nanofiber to be in the range of 2.90 ± 1.4 GPa and 180 ± 60 GPa, respectively [1], while others approximate the electrical resistivity to 1×10^{-4} $\Omega \cdot$m [2]. Besides having properties comparable to their counterpart carbon fibers, carbon nanofibers (CNFs) are less expensive and simpler to process than other forms of carbon, making them an ideal constituent for the fabrication of next generation advanced materials.

Motivated by the science and technology of particles, the development of polymeric composites containing these unique nanoscale constituents–CNFs–create a new set of material challenges related mostly to their processing in polymers and their characterization at both atomic and macroscopic level. Even though a reduction in reinforcement size from microscale to nanoscale dimensions offers great opportunities to engineer multifunctional materials with tailored properties, a number of critical issues need to be overcome in order to make the best use of CNFs in composites. These involve: 1) dispersion/impregnation of CNFs in matrix; 2) spatial orientation of CNFs in a composite; and 3) chemical compatibility between CNFs and matrix. In general,

challenges like these are faced when fabricating advanced materials containing other carbon forms (carbon nanotubes, graphene, etc.) as well.

Over the past few years, a number of scientists have worked around different strategies to mitigate these material and processing issues. They have used techniques such as sonication, functionalization, calendering, etc., to directly incorporate nanoparticles into polymer and produce nano-engineered composites with enhanced properties. Up to some extent, they found that untangling nanoparticles in a matrix was an effective way to allow load transfer from the matrix to the particles when subjecting a composite to external loading. Nevertheless, the high nanoparticle aspect ratio (diameter/length) caused difficulties at maintaining uniformly dispersed nanomaterials during matrix cure. These tended to re-aggregate due to their own instability–high van der Waals forces–negatively impacting the material properties of the resulting composite.

In view of this, researches have used covalent/non-covalent functionalization methods as means for improving nanoparticle stability and compatibility with matrix. On the down side, the harsh chemical conditions required to add functional groups on the nanoparticles' surfaces caused a reduction in their aspect ratio, detrimental to material properties. However, the impact obtained through these approaches translated into composite with promising properties. The presence of chemical groups on the nanoparticles' surfaces, in the case of covalent treatment, helped improve the interaction with matrix by forming chemical links and preventing both re-agglomeration and slippage of particles.

To some degree of success, these techniques can be used to fabricate composites with relatively low nanoparticle content. As the nanoparticle volume fraction increases, an additional processing difficulty arises due to rise in viscosity. Thus, other processes are essential to effectively fabricate composites with high nanoparticle content. A unique method to do this is by

deliberately binding together nanoparticles, such as carbon nanofibers/nanotubes, to form a thin film of discontinuous nanoparticle entangled network, which is commonly known as buckypaper [3, 4]. This indirect approach permits the creation of composites with high nanoparticle content but without processing difficulties due to high viscosity. Furthermore, it allows the buckypaper to be externally impregnated with polymer matrix, assembled, and cured to form a nano-engineered composite with properties orders on magnitude higher than those of neat polymer matrix.

Because of a combination of high aspect ratio and high flexibility, the intensified interatomic forces (van der Waals forces) between nanoparticles cause their agglomeration into close-packed bundles [5, 6]. When assembled, these bundles form a mat–buckypaper–with tensile strength typically in the 5-30 MPa range [7-10] and sufficient mechanical stability to be handled as a free-standing thin film. Yet, the microscopic discontinuity between nano-scale filaments in buckypaper leads to inter-filler junctions, which adversely affect its mechanical, electrical, and thermal properties [11, 12]. Particularly, as reported by Tawfick et al. [13], the electrical conductivity of nanotube-based buckypaper could decrease at least two orders of magnitude with respect to the theoretical conductivity of a single nanotube because of inter-filler junction. Furthermore, the inherent nature of the buckypaper's fabrication process–usually involving multiple steps–has been found to produce significant gap between particles, resulting in papers with large quality variation. Hence, there is a need to fabricate high quality nano-engineered thin films by establishing control processes to reduce inter-filler junctions, improve interactions between particles, and ultimately deliver materials with superior properties.

1.2. Research Objectives

This investigation describes the processing and characterization of dense nano-engineered thin films fabricated by a unique two-step approach, which combines solution filtration and mechanical compression through a rolling process. The findings are intended to aid in the creation of next generation advanced materials.

Based on the motivation of this research, the specific objectives are as follows:

1. Develop a process to fabricate dense functionalized CNF thin films

2. Characterize the CNF thin film bulk density and change in surface morphology caused by the rolling process

3. Evaluate the CNF thin film strength and electrical conductivity as well as investigate their possible correlation with thickness and density

The structural organization of this work is presented in the following manner: Chapter 1 introduces the subject by discussing the main issues associated with manufacturing of nano-engineered composites and thin films as well as presents the objectives of this investigation. Chapter 2 reviews the research related to the technology of carbon nanotubes/nanofibers. The synthesis, morphology, and properties of these nanoparticles are studied along with processing and characterization techniques for fabricating thin films (buckypaper). Chapter 3 describes the functionalization scheme for chemically modifying CNFs and addresses the synthesis of nano-engineered thin films. Chapter 4 reports the physical, mechanical, and electrical characterization of nano-engineered thin films and describes their microscopic change in surface morphology due to mechanical compression. Finally, Chapter 5 presents the conclusions of this investigation by stressing the importance of mechanical compression during the fabrication of nano-engineered thin films.

CHAPTER 2

LITERATURE REVIEW

2.1. Carbon Nanotubes

Since the mid-80s, the recognition of Buckminsterfullerene (C_{60}) as a form of carbon has blossomed the Carbon Science in countless fields of research. Fullerene provided exhilarating insights into nano-scaled architectures comprising sp^2 hybridized carbon atoms and how these structures resulted in new materials with fascinating and advantageous properties. Carbon nanotubes (CNTs) constitute the clearest instance.

While Oberlin et al. [14] unknowingly produced the first images of a nano-sized filament resembling a single-walled carbon nanotube using transmission electron microscopy in 1976, the emerging field of CNT was marked by Iijima et al. in 1991 [15]. His first unambiguous observations of what seemed to be cylindrical carbon forms of tens of nanometers (carbon nanotubes) opened a new avenue in nanotechnology. Unlike diamond, a carbon allotrope with atoms arranged in a rigid tetrahedral network (Sp^3 hybridized), carbon nanotubes comprise an assembly of Sp^2 carbon molecules hexagonally arranged to form coaxial graphitic sheets (2-50 sheets) spaced by 3.4 angstroms. Transmission electron micrographs of nanotubes are shown in Figure 1. Eventually, these forms of carbon were named multi-walled carbon nanotubes (MWCNTs).

Shortly thereafter in 1993, two separate investigations (Iijima et al. [16] and Bethune et al. [17]) divulged the structure of a newly recognized carbon structure−single-walled carbon nanotubes (SWCNTs). Both reports not only described the structure of single-shell carbon nanotubes grown by electric arc discharge with metal catalyst (iron, cobalt), but also measured the

diameter of single-shell nanotubes to be close to 1−1.2 nm. Electron diffraction pattern and

electron micrograph of a single-shell nanotube are illustrated in Figure 2.
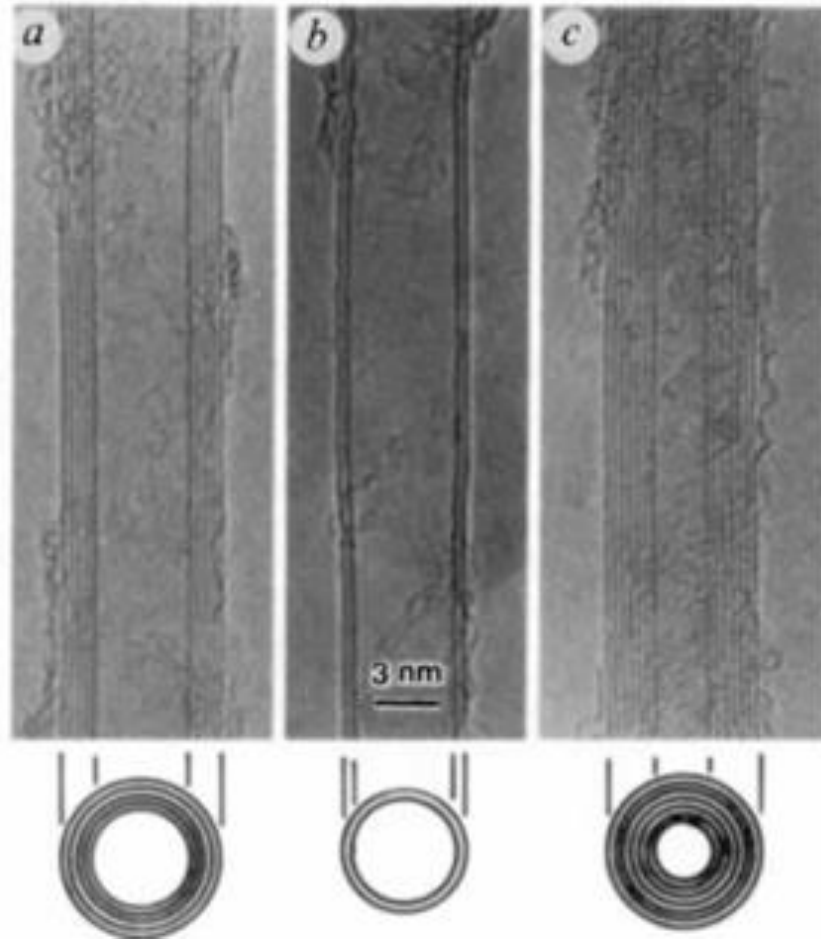
Figure 1. Transmission electron micrographs of the CNTs reported by Iijima et al. [15]. Symmetrical parallel lines define the projections of graphitic sheets coaxially arranged. (a) Represents a tube of five graphitic sheets, diameter 6.7 nm. (b) Represents a two-sheet tube, diameter 5.5 nm. (c) Represents a seven-sheet tube, diameter 6.5 nm, with the smallest inner tube diameter (2.2 nm) [15].
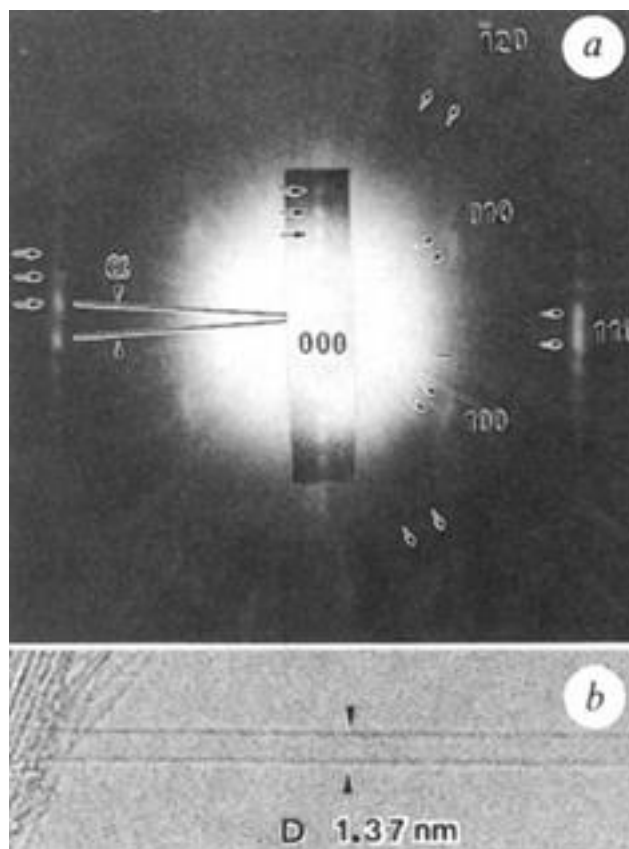
Figure 2. (a) Electron diffraction pattern taken from a single-shell nanotube (diameter 1.37 nm). (b) Electron micrograph of the same nanotube.

2.1.1. Growth of Carbon Nanotubes

A wide variety of techniques has been utilized to create CNTs. The most popular ones involve: arc discharge [15-20], laser ablation [5, 21-23], gas-phase catalytic growth [24], electrochemical growth in condensed phase [25-27], and chemical vapor deposition (CVD) [28-33].

The arc discharge technique, in which CNTs were initially grown, is linked to the fullerene synthesis [34]. In this method, CNTs are formed by evaporating pure graphite rods while applying an AC voltage in an inert environment followed by a DC arc voltage. The evaporated anode produces soot of fullerenes while a small part of evaporated anode that deposits on the cathode

contains CNTs, mostly MWCNTs [15]. MWCNTs with the smallest innermost tube have been produced by this method in pure hydrogen (H_2) gas [35, 36] while the mass production of MWCNTs has been realized in helium (He) atmosphere [37, 38]. Using a growing technique similar to that for MWNCTs but with metal catalysts (Fe, Mo, Co, Ni, etc.) incorporated into the graphite anode rod, SWCNTs were synthesized in the form of soot [16, 17, 39]. Large-scale production of SWCNTs has also been achieved using a bimetallic catalyst in a mixture of H_2/Ar gas [39].

In laser ablation, initially intended for fullerene synthesis [5, 40], a laser beam aims to a carbon source composite doped with metal catalysts located in the middle of a reactor furnace. The carbon source vaporizes in high-temperature Ar gas to form SWCNTs. The main benefits of this method include: high-quality SWCNT production and diameter control. SWCNTs with negligible structural defects and surface contaminants (amorphous carbons, residual catalyst, etc.) have been made by this method together with purification processes based on hot air or chemical oxidation [41, 42]. Control over the nanotube diameter has been attained by adjusting the furnace temperature, metal catalyst, and gas flow rate [43-45]. High furnace temperature results in nanotubes with large diameters [43]. Alloy catalysts such as Ni-Y yield nanotubes with large diameters, whereas other catalysts, such as Rh-Pd, etc., produce nanotubes with reduce ones [45, 46]. Flow rate has been found to affect the diameter distribution, suggesting a sluggish growth process [44].

Up till now, both synthesis methods (arc discharge and laser ablation) are capable of growing high yield CNTs. However, the downside of these techniques is related to processing limitations due to a finite carbon source, which restricts the volume of nanotubes produced as well

as increases the direct production costs. Furthermore, formation of by-products such as encapsulated metal particles and amorphous carbon are other issues involving these processes.

Gas-phase catalytic growth and chemical vapor deposition (CVD) are currently the most predominant techniques used to grow CNTs, in which a hydrocarbon gas is thermally dissociated in the presence of active metal catalyst(s). In contrast to arc discharge and laser ablation, these are promising and economical methods to synthesize CNTs. First, their simple operation makes them favorable options to produce CNTs at large-scale. Technically, in their simplest setup, they only need a tubular reactor, an oven, and a mass flow controller to supply the hydrocarbon gas mixture. Second, they provide better control over processing parameters (e.g. temperature and carbon concentration on the catalyst's surface) during catalyst treatment or nanotube growth to influence the yield and the quality of CNT produced. Furthermore, the versatility of the methods enables the use of many hydrocarbon sources in any stage (solid, liquid, gas) as well as various substrates, permitting CNT grown in multiple forms (power, aligned, entangled, etc.).

CVD is a technique that has been applied to produce carbon filaments since the mid-twentieth centuries [47, 48]. By a method resembling that used by Iijima et al. [15], Endo et al. [49] reported the formation of CNTs from the pyrolysis of benzene at more than 1000 °C; others grew MWCNTs at 700 °C in an acetylene atmosphere [50]. Both methods used Fe particles as catalyst. Other approaches have considered decomposing high-carbon-content gases such as methane [50], ethylene [51, 52], and other hydrocarbons to grow MWCNTs. By dissociating carbon monoxide (CO) at 1200 °C in Mo catalyst particles, Dai et al. [53] produced the first SWCNTs by CVD. Later reports described the SWCNT production from methane, ethylene, and benzene using different catalysts [54-56].

9

In a typical CVD process, a hydrocarbon vapor passes through a tubular reaction furnace containing a catalyst material at elevated temperature (600-1200 ℃) to allow hydrocarbon decomposition. CNTs grow over the catalyst surface and they are collected upon cooling of the system. For liquid hydrocarbons (benzene), the liquid is first evaporated in a heated flask and the evolving vapor is then fed in the furnace together with an inert gas. Vaporization of solid hydrocarbon (naphthalene) is obtained by placing it in a low-temperature furnace before putting it inside a reaction furnace.

The growth of nanotubes (SWCNTs/MWCNTs) is governed by the catalyst particle size. Transition-metal nanoparticles (Ni, Fe, Co) of control size can be utilized to grow nanotubes of specific diameter [57, 58]. A particle size in the range of a few nanometers yields SWCNT formation, whereas particles in the tens of nanometers favor MWCNT growth. Despite controlling various hydrocarbon sources and catalysts to make CNTs of a particular structure (single-/multi-walled) in CVD, temperature is another imperative parameter for nanotube growth in this method. Broadly speaking, low temperature (600-900 ℃) in the CVD furnace favors MWCNT growth while higher reaction temperatures (900-1200 ℃) yield SWCNTs.

While CVD involves the use of transition-metal catalyst to induce CNT formation from hydrocarbon decomposition; in the gas-phase growth, CNTs' catalysts form *in-situ* by dissociating Fe at 800-1200 ℃ in the presence of CO. The liberation of metal particles *in-situ* catalyzes the synthesis of CNTs.

Electrochemical growth is a process to make CNTs in liquid phase. CNTs grow when a DC electric field is applied to graphite electrolytes immersed in LiCl. While the DC current flows through the system, the carbon atoms dissolve in the salt and they are isolated in a hexagonal array

to form CNTs. The lack of controllability and complexity of the reaction, however, limits its applicability for mass production.

2.1.2. Morphology and Properties of Carbon Nanotubes

CNTs have become the symbol of a new nanotechnology era. Their manufacturing and characterization techniques have evolved substantially since reported in 1991. With typical diameters in the range of 1-50 nm and lengths of many microns, CNTs are frequently visualized as the insertion of very small carbon fibers into fullerenes. Their morphology comprises one or more coaxial layers of graphene rolled over any orientation along the two-dimensional lattice vector (m,n) to form a tube-like structure (SWCNTs/MWCNTs). The orientation of the hexagonal lattice with respect to the tube axis defines not only the nanotube's chirality or helicity [59], but also their diameter and properties [59, 60].

Chirality or helicity is mathematically described in terms of the chiral vector, $\vec{C}_h$, and the chiral angle, θ. $\vec{C}_h$ defines the direction in which the graphene sheet rolls over and it is described in terms of two integers (n,m) along the hexagonal lattice and two unit vectors ($\vec{a}_1$, $\vec{a}_2$) according to the following equation: $\vec{C}_h = m\vec{a}_1 + n\vec{a}_2$. θ defines the chiral vector aperture with respect to the zig-zag structure of graphene [20, 61]. When θ is either 0º or 30º, the boundary apertures for $\vec{C}_h$ in CNTs, the CNT helicity is referred to as armchair or zig-zag structure, respectively. In the former structure, the honeycomb lattice (*n,n*) lies perpendicular to the tube axis; while in the latter structure (*n*,0), the carbon-carbon bonds lie parallel to the tube axis. All other lattice conformations of the form (*n*, *m*, where *m*≠0 and *n*) are identified as chiral nanotubes [62]. A schematic representation of the non-chiral and chiral atomic arrangements of nanotubes is shown in Figure 3. In his review, Terrones et al. [20] described an expression to calculate the tube diameter from

$\vec{C}_h$ as $d = \frac{a\sqrt{m^2+mn+n^2}}{\pi}$, where a corresponds to the lattice constant in the graphene sheet ($a = 1.42 \times \sqrt{3}$ Å).
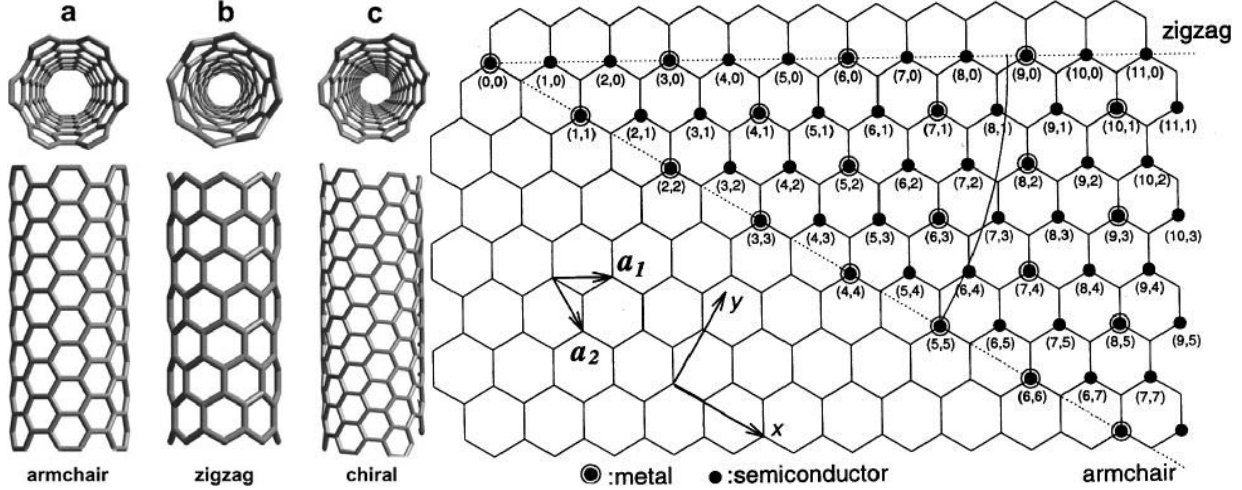
Figure 3. (Left) Molecular models of non-chiral and chiral SWCNTs: (a) armchair, (b) zig-zag, and (c) chiral. (Right) Schematic diagram of chiral vector and chiral angle in the honeycomb lattice of graphene [20].

Of important note is that theoretical investigations on the CNT electronic properties postulate that all armchair and zig-zag (those with honeycomb lattices (*m*, *n*) multiple of three) nanotubes are metallic in nature [63, 64]. Later studies, nevertheless, suggest that the metallic or semi-conductive behavior of CNTs depends on their conformational chirality [65].

Studies on axial stiffness, bending, and torsion of nanotubes with respect to chirality have indicated that chiral CNTs exhibit a unique asymmetric torsion characteristic relative to the left/right twist, while the tensile modulus remains unaffected [66]. This behavior, however, is absent in armchair and zig-zag tubes. Furthermore, molecular dynamic simulations have shown that chirality has little influence on the elastic properties of CNTs, and that the high deformation of nanotubes produces abrupt changes in morphology [67]. Such changes in patterns have been described in terms of the Stone-Wales transformation: a defect caused by a reversible

12

rearrangement of atoms in the nanotube honeycomb lattice, forming a structure of two heptagon-pentagon pairs, as illustrated in Figure 4. Quantum mechanics studies have shown that the fracture mechanism of nanotubes occurs due to reconfiguration of carbon bonds lying within the pentagon rings [68]. Likewise, the new defects created by the Stone-Wales transformations may considerably affect the individual properties of CNTs. As demonstrated by molecular dynamics, the nanotubes' load carrying capabilities depend not only on the density of defects and location of imperfections in the lattice, but also on the size of the tubes [69]−defects in small tubes are more detrimental than in large ones. Further simulation studies have confirmed that defect-free nanotubes have higher elongation than flawed ones, and that the nanotube stiffness is independent of the density of defects at slow loading speeds only [70].
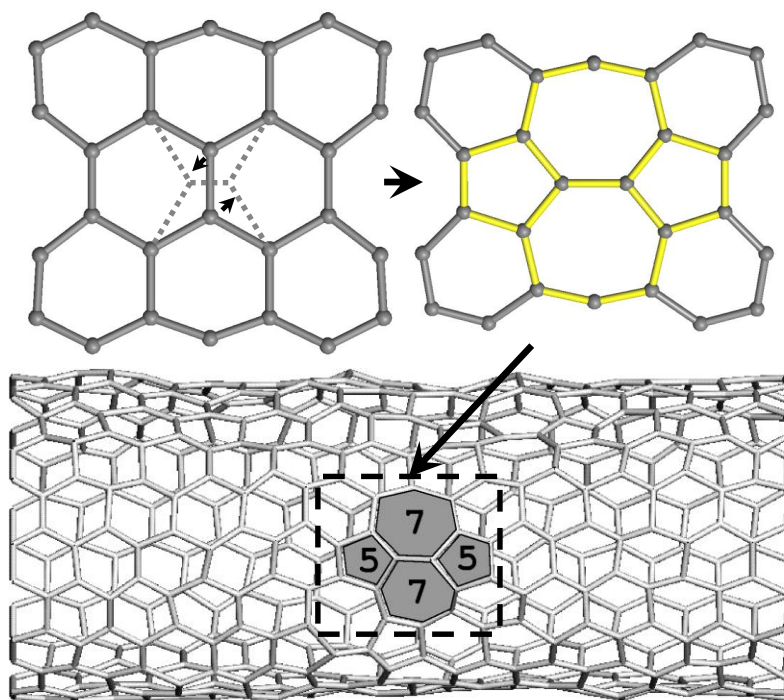
Figure 4. Top: Stone-Wale diatomic interchange in the hexagonal wall of a nanotube [71]. Bottom: Stone-Wales defect at 2000 K and 10% strain [72] .

2.2. Carbon Nanofibers

Carbon nanofibers are an important class of graphite-like materials. Although lacking the structural perfection of CNTs, particularly those made of a single sheet of graphene, vapor-grown carbon nanofibers (VGCNFs) or simply carbon nanofibers (CNFs) are thought to have similar mechanical and thermal properties. Historically, the creation of CNFs goes back to the development of submicron-sized carbon filaments from hydrocarbon sources in 1889 [73]. Until the 1970s, the CNF formation was viewed as an undesirable by-product during the production of carbon fibers. Enthusiasm over the potential utility of CNFs, however, has grown over the years. Researchers have come to realize that fiber-like materials are of great scientific and practical importance. By combining high surface area and exceptional mechanical properties, CNFs can be used to fabricate advanced composites for a wide variety of applications. In their simplest form, CNFs are sp^2-based filaments with diameter and length in the nanometers and micrometers range, respectively. Because of their overall dimensions, they are also characterized by high flexibility and aspect ratio (250-2000). Reviews about manufacturing and properties of vapor-grown carbon fibers and VGCNFs are found in [74-76].

2.2.1. Synthesis of Carbon Nanofibers

Catalytic CVD is one of the most widely used methods for growing CNFs. It allows production at large-scale and at low cost. This method involves the catalytic dissociation of a carbon feedstock (hydrocarbon or carbon monoxide) exposed to a metal (Fe, Ni, Co) or alloy (Ni-Cu, Fe-Ni) catalyst in a reactor kept at 500-1500 °C. During this process, a carbon source is absorbed and decomposed on certain faces of a metal/alloy, followed by diffusion of carbon atoms through a catalyst particle that precipitates at other faces in a fibrous form. Depending on the catalyst nature, carbon feedstock, and reaction conditions, CNFs with different degree of

14

crystalinities and various conformations (straight, twisted, and helical) are formed [77]. Further morphological modification of CNFs is accomplished by recrystallization of graphitic planes (outer layers) through graphitization treatment. This process produces CNFs with not only higher mechanical and electrical properties due to rearrangement of the turbostratic layer along the fiber direction, but also lower physical properties caused by formation of discontinuous conical crystallites [75]. In his studies, Tibbets et al. [75] reported that 1500 °C and 1300 °C were the best heat treatment temperatures to achieve CNFs with optimum performance in terms of mechanical and electrical properties, respectively.

2.2.2. Morphology and Properties of Carbon Nanofibers

Unlike the sole cylindrical structure of CNTs, CNFs comprise a duplex carbon layer in their pristine form. Regularly truncated conical graphitic sheets of high-crystallinity stacked at 19-85° relative to the longitudinal fiber axis form the inner layer [78], while a graphene turbostratic core co-axially oriented along the filament length and surrounding the inner layer forms the outer layer. Depending on the graphene planes' stacking arrangement, CNFs with different morphologies are formed: cup-stacked [79], bamboo-like [80], and parallel [81]. Parallel nanofibers comprise cylindrical graphitic layers coaxially oriented parallel to the fiber axis. Structure-wise, these fibers resemble MWCNTs. Cup-stacked/bamboo fibers, on the other hand, have the truncated cone-shaped structure described above. Studies suggest that the spacing between adjacent graphene planes is around 0.34 nm, which coincides with the interlayer spacing found in MWCNTs [82]. Transmission electron micrographs of a CNF with various graphene layers are depicted in Figure 5.
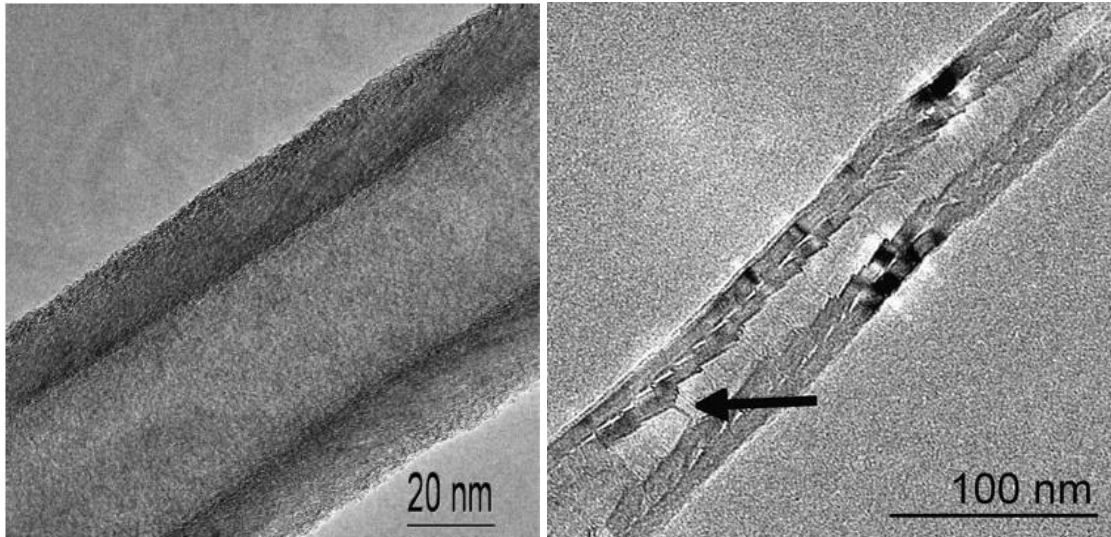
Figure 5. Transmission electron micrographs describing: (1) the structure of a CNF with a cylindrical hollow core −one graphene layer (left) [75]; (2) the structure of a CNF with both cylindrical hollow core and turbostratic layers [81].

As in nanotubes, the mechanical properties of CNFs depend on their morphological arrangement −changes in inner/outer layers, conical angle, and orientation of graphene panels. Through *in-situ* experiments with a microelectromechanical system (MEMS) device, the tensile strength and elastic modulus of cup-stacked CNFs have been estimated at 2.90 ± 1.4 GPa and 180 ± 60 GPa, respectively [1]. The MEMS-based platform used to directly quantify the tensile strength and elastic modulus of cup-stacked CNFs is shown below (Figure 6).

Experimental studies have also proposed that CNFs behave like carbon fibers when subjected to post-treatment methods. Reports have shown that temperature treatment negatively impacts the tensile strength of CNFs while benefits their elastic modulus [1, 2]. The increase in modulus and decrease in strength, caused by high-temperature treatment, confirm that heat-treated CNFs undergo morphological transformation due to degradation of the outermost turbostratic layer and graphitization of inner planes, which degrade their tensile strength.
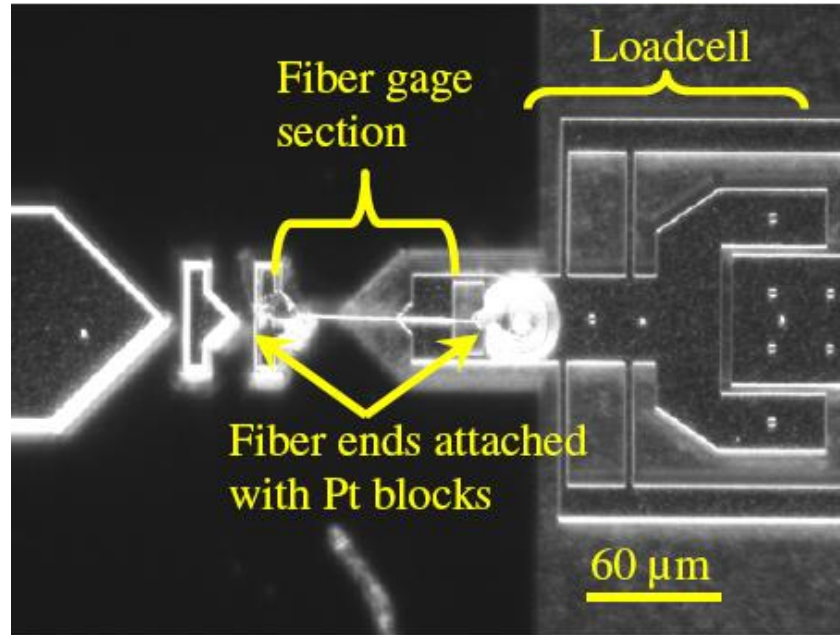
Figure 6. MEMS-based platform used for direct measurement of CNF tensile properties [1].

Since CNF is an allotrope of carbon with structure and properties closely related to other forms of carbon, it is convenient to establish a relationship between fibrous carbon materials, specifically nanoparticles and carbon fibers. Being an essential class of graphite material, carbon fibers act as a bridge between nanoparticles and typical bulky carbon materials. A comparison between physical and mechanical properties of carbon fibers, CNFs (VGCNFs), and CNTs is reviewed in Table 1 [2]. Compared to conventional carbon fibers, CNFs/CNTs exhibit superior properties due, in part, to increased aspect ratio and decreased presence of structural defects. In fact, the nano-/micro-size dimensions of these particles increase the surface area available for interaction within a structure, making them ideal reinforcement agents for various composite applications.

TABLE 1

PROPERTIES OF CARBON FIBERS, CNFS, AND CNTS [2]

Properties	Carbon Fiber	CNF	SWCNT	MWCNT
Diameter (nm)	7300	50-200	0.6-1.8	5-50
Density (g/cm^3)	1.74	1.75	1.33-1.4	1.3-2.25
Aspect ratio	440	250-2000	100-10000	10-10000
Tensile strength (GPa)	3.8	2.92	50-500	10-60
Tensile modulus (GPa)	227	240	1500	1000

Regarding electrical properties, the high conductivity (reciprocal of resistivity) of CNFs makes them favorable candidates for formulating conductive polymers. Experimentally, the electrical resistivity and density of CNFs have been measured at 1×10^{-4} $\Omega \cdot$m [2] and 1.95-2 g/cm^3 [2, 83], respectively. Nanofibers, in their pristine form, normally contain a layer of amorphous carbon (impurity) which reduces the nanoparticle's conductivity. However, through post-processing methods like heat treatment, researchers have found ways to eliminate this impurity and increase the crystallinity of CNFs. By carbonizing and graphitizing CNFs at 1200 °C and 2800 °C, Endo et al. [84] showed that the volume resistivity of nanofibers could decrease to 10^{-3} and 10^{-4} $\Omega \cdot$m, respectively.

2.2.3. Post-processing of Carbon Nanotubes & Carbon Nanofibers

Due to their strong interatomic forces (van der Waals forces) and high surface area, nanoparticles like CNTs/CNFs tend to group together and form aggregates difficult to separate. If they are not broken apart, these agglomerates can compromise the integrity of nano-engineered composites and deter the use of nanotubes/nanofibers as a possible reinforcement agent. In order for load transfer to be effective, there must coexist: 1) a uniform particle distribution and 2)

18

improved filler interaction within a matrix. These parameters are particularly imperative, because individual nanotubes/nanofibers provide the highest interfacial area for stress transfer to occur. A common approach to improve the fillers' dispersion and interaction within a matrix is by chemically altering the nanoparticles' surfaces through either a non-covalent or a covalent functionalization scheme. Either method intensifies the nanoparticles' surface energy, creating repulsive forces needed to stabilize individual tubes/fibers in a medium. Formation of chemical linkage between tubes/fibers and polymer depends normally on the type of covalent treatment performed. For instance, tube functionalization with amine has been shown to improve the mechanical properties of composites as a result of the high affinity of amine moieties with epoxy [85].

Up till now, a number of covalent functionalization schemes have been developed for grafting moieties such as hydroxyl [86], carboxylic acid [87, 88], amine[89], pyrene [90], and epoxide [91] onto CNTs/CNFs with various levels of success [92, 93]. Among all, the most widely used scheme is the open-end approach through an oxidation route, normally by refluxing with nitric acid. This functionalization technique shortens nanotubes/nanofibers and forms carboxylic acid end groups, which can be successively converted into other organic groups through conventional condensation reactions. Lakshminarayanan et al. [87] exposed VGCNFs to nitric acid for various time periods to analyze changes in the nanofibers' atomic structures due to oxidation. After oxidizing the nanofibers for 90 minutes, the surface atomic oxygen increased from 6% to 22% without significant morphological damage, and the fibers became soluble as a result of an increase in wettability. Lachman et al. [94] demonstrated that toughness in epoxy based composite could increase by adding MWCNTs functionalized with carboxylic acid and amine. The authors credited this result to improvement in both dispersion quality and interfacial interaction. Seyhan

et al. [95] investigated the fracture toughness of epoxy-based polymers reinforced with 1 wt% silane-treated CNFs and found an increase in toughness of 12%. Prolongo et al. [96] used a multi-step method to graft amine to CNFs and investigated the properties of composites reinforced with these particles. An enhancement in elastic modulus was attributed to better nanofiber distribution in the matrix when coupling chemical functionalization, sonication, and high shear mixing.

The main drawback of covalent functionalization, however, is the deterioration of the π-conjugation present in the sp^2 hybridized structure of nanotubes/nanofibers. Although its impact is limited in terms of mechanical and, maybe, thermal properties, the disruption of the π-bond greatly affects electrical properties. With each covalent functionalization, moieties are incorporated onto the end caps or size walls of CNTs/CNFs, resulting in significant electron scattering.

While the covalent functionalization scheme requires strong chemicals to oxidize the nanoparticles' surfaces, the non-covalent functionalization method uses a mixture surfactant-solvent to tune the nanoparticles' interfaces and create uniform particle dispersion. Surfactant is an organic solution consisting of both hydrophobic and hydrophilic groups, basically an amphiphilic micelle. According to its use, it is classified in four categories: anionic, nonionic, cationic, and amphoteric or zwitterionic. When used as a dispersing agent during the fabrication of nano-engineered composites, the hydrophobic group in surfactant interacts with particles through absorption mechanisms while the hydrophilic part interacts with polymer throughout secondary bonding–hydrogen bonding. The induced steric or electrostatic repulsion among nanoparticles occurs as a result of surfactant absorption, which counterbalances van der Waals attractions; therefore, the nanoparticles repel and stabilize forming a colloidal system. Note that the decrease in surface tension due to surfactant absorption on the nanoparticle's surface prevents

the formation of agglomerates also. Through mechanical stirring, Gong et al. [97] dispersed nanotubes in epoxy resin with the aid of a non-ionic surfactant. Results showed considerable improvement in glass transition temperature and elastic modulus for composites with 1 wt% nanotubes. The authors also pointed out difficulties in achieving uniform nanoparticle distribution by using surfactant as processing aid. Later, Geng et al. [98] observed that the hydrophobic-hydrophilic nature of surfactant produced bridging effects between nanotubes and epoxy. Such effects were responsible for enhancing the thermomechanical, mechanical, and electrical properties of composites containing nanotubes treated with a nonionic surfactant (Triton X-100).

The non-covalent functionalization is predominantly attractive when structural nanoparticle damage is of concern. The physical absorption of surfactant tends not to alter the distinctive structure of nanotubes/nanofibers or their π-bond conformation, particularly important for electrical properties [99]. Even though a growing number of literatures present new strategies to enhance the interaction and compatibility of nanoparticles with polymer, the argument of whether pristine or functionalized nanotubes/nanofibers can be used to create the next generation of advanced composites is yet to be solved. A more comprehensive study involving each of these carbon allotropies is necessary in order to understand the structure-processing-property relationship of nano-engineered materials.

2.3.   Processing of Carbon Nanotubes & Carbon Nanofibers

The recent interest in developing advanced materials by taking advantage of the unique properties of nano-scale carbon particles (CNTs/CNFs) has led to extensive and diverse research on how to effectively embed these exceptional fillers into different compounds (polymers, ceramic, etc.). Like in fibrous composites, the properties of nanoparticle-based materials depend

on their constituents (CNT, CNF, matrix, fiber, etc.), their interaction (fiber/matrix) as well as their geometrical arrangement (orientation, dispersion, and concentration).

As the overall size of a particle becomes smaller, both surface area and van der Waals forces intensify. As a result of these, CNTs/CNFs tend to self-associate into micro-scale clusters difficult to disrupt. Such agglomerates need to be broken apart in order to promote interaction between constituents and not to compromise or limit the composite performance. Over the years, significant effort has been devoted to developing mechanical and chemical strategies to break these agglomerates and improve dispersion of nanoparticles within a matrix. These strategies include, but are not limited to: covalent/non-covalent functionalization, ultrasonic dispersion, mechanical shear mixing, solution and melt blending, in-situ polymerization, or a combination of these. In particular, chemical techniques–covalent/non-covalent functionalization–inhibit nanoparticles' re-agglomeration by modifying their surface energy, wetting, and adhesion. Although both chemical and mechanical methods produce the physical separation of nanotubes/nanofibers, they tend to cause structural damage and reduce aspect ratio. On the positive side, however, remarkable enhancement in properties has been achieved by directly embedding either CNTs or CNFs into polymers through these processes.

A standard procedure to disperse nanoparticles in a medium is by using an ultrasonic device or sonicator. This tool applies cavitation (formation and implosion of bubbles) induced by ultrasonic waves of high frequency to a fluid (water). The agitation produced in the liquid generates high forces on a container–normally a glass beaker–filled with a mixture of nanomaterial (CNTs/CNFs) and solvent (water, alcohol, etc.). This action produces nucleation of bubbles at the nanoparticle surface, which rapidly pushes the nanoparticles apart, breaks the agglomerates, and forms a well-dispersed particle solution.

Besides cavitation in liquid, there is another phenomenon occurring at high intensity sonicaton over prolonged period of time: localized heating. This is the result of the continuous collapse of bubbles which produces a high concentration of energy due to conversion of kinetic energy of liquid to heat. Consequently, a balance between amplitude and time is essential to prevent irreversible damage on the structure of nanotubes/nanofibers and effectively obtain a homogenous particle solution. There are mainly two types of ultrasonic dispersion approach: horn (tip) and bath. The difference is basically the way in which a nanoparticle-solvent mixture is subjected to cavitation. In the former, the output tip of the horn is place in direct contact with a treated medium (e.g. nanoparticle-solvent mixture); while in the latter, a solution contained in a glass beaker is placed in a cup-horn filled with water. The ultrasonic waves are transmitted from the water to the solution indirectly, since the sonotrode is in contact with water.

Sonication is a very useful technique and, in some cases, it has been utilized to remove impurities and to reduce the nanoparticles' length. SWCNTs synthesized by laser-vaporization have been purified to more than 90% by ultrasonicating a methanol/nanotube mixture during filtration [100]. By combining bath sonication for 6 hours and air oxidation at 500 ºC, Shimamoto et al. [101] reduced the length of cup-stacked carbon nanotubes and activated their structure chemically without significant damage. The authors improved the solubility of particle in distillate water because of a reduction in length and formation of active end planes on the outer surface of nanotubes.

Ultra-sonication has also been used as a tool to fabricate nanoparticle-based composites. Na et al. [102] investigated the effect of different sonication profiles on the electrical properties of low-density polyethylene (LDPE)/carbon nanotube composites. At a concentration of 20g/200ml

of MWCNT/LDPE, they obtained an enhancement in electrical properties and pointed out that a better dispersion was possible by augmenting the sonication amplitude.

An alternative approach to incorporate nanotubes/nanofibers into polymers is shear mixing–calendering. This technique permits the direct dispersion of nanoparticle in a host matrix by mechanically breaking the clusters apart. While a moderate increase in mechanical properties has been reported [103], the method is restricted to small particle volume fraction in the polymer. As the particle content increases, the viscosity of the matrix rises considerably due to the high nanoparticle specific area (Figure 7), hindering the manufacturing of nano-engineered composites. Although temperature increase is a mean for reducing matrix viscosity during composite preparation, there is a risk of curing during processing that will ultimately raise viscosity. As such, this shear process is usually constrained to low particle content in order to avoid the use of temperature and prevent rise in viscosity during fabrication of nanoparticle-based composites.

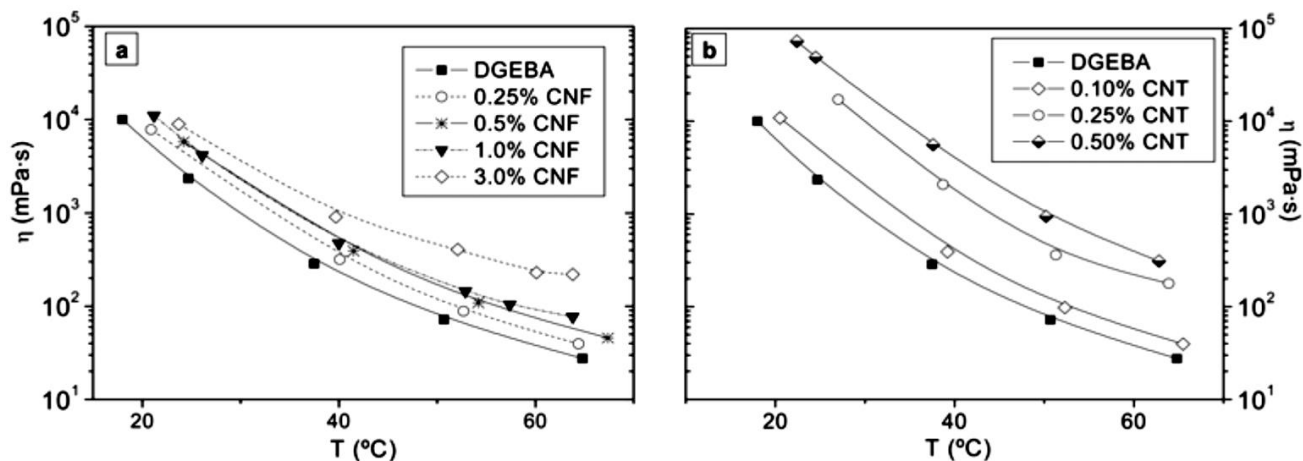Figure 7. Viscosity change with respect to temperature for epoxy
monomer and various content of (a) CNFs and (b) CNTs [104].

Using a calendering approach, Gojny et al [103] obtained improvement in strength and toughness after dispersing 0.1 wt% of double-walled CNTs in epoxy resin. Later on, Thostenson et al. [105] found similar results, which reaffirmed the hypothesis that fracture toughness of neat

epoxy could improve significantly by adding a well-dispersed low-concentration of CNTs. Moreover, the authors achieved a conductive percolation network in the compounds as a consequence of high nanotube aspect ratio at concentrations of less than 0.1 wt%.

Besides shear mixing, numerous processes have been utilized to incorporate nanotubes or nanofibers into matrix. By taking advantage of the matrix polarity, Lafdi et al. [106] functionalized CNFs with compatible moieties to increase the particle-matrix interaction and correlated mechanical, electrical, and thermal properties of nanocomposites to CNF treatment time. While their findings showed remarkable improvements in flexural strength and modulus for composites with CNFs treated for 12 minutes, there was an increase in electrical resistivity for composites containing CNFs treated for longer time due to higher oxygen content. Bortz et al. [107], on the other hand, investigated the monotonic and dynamic fracture behavior of CNF-based epoxy composites prepared with a laboratory mixer. The authors improved the material resistance to fracture as well as fatigue performance but they pointed out the need for a much more effective dispersion method. The presence of CNF agglomerates prompted accelerated crack growth. By combining several techniques–covalent functionalization, sonication, shear mixing–Guzman et al. [108] narrowed down several processing parameters to add CNTs into epoxy/phenolic-base compound and create composites with superior strength. Improvement at the nanotube-matrix interface and uniform nanotube dispersion resulted in a tremendous increase in compressive and lap shear strength of 60% and 100%, respectively, compared to the neat compound. Their results also emphasized the importance of establishing control processes during fabrication of nanotube-based composites.

2.4. Processing of Nanoparticle-based Thin Films

While the aforementioned methods directly integrate fillers at low weight fractions into matrix, there are other indirect routes that permit composite fabrication with high nanotube/nanofiber content. These encompass the assembly of carbon nanomaterials into a thin film form, often known as buckypaper. This paper can then be permeated with polymer to obtain a nano-engineered composite after curing at a predefined temperature.

Carbon-based thin films or buckypapers are an assembly of discontinuous and randomly oriented nanomaterials (CNFs, SWCNTs, MWCNTS, etc.) [4, 109, 110]. Their initial production in 1998 [6] allowed the transformation of individual carbon nanoparticles into a macroscopic element with paper-like morphology and measurable physical properties. As a bulk composite, their properties (mechanical, electrical and thermal properties, to name a few) depend not only on the random orientation of nanoparticles as well as their numerous interactions (inter-filler junctions), but also on the nanoparticle geometry, structure, morphology, and presence of polymer binder. While solution filtering is the most conventional method used to fabricate buckypaper, new methods have emerged in recent years. These include: CVD growth [111-113], electrophoretic deposition [114, 115], drop drying [7, 116], Langmuir-Blodgett [117-119], and self-assembly [120, 121]. Liu et al. [122] converted highly amorphous bundles of nanotubes into free-standing mats (Figure 8) by vacuum filtering a colloidal suspension of nanotube-water-surfactant (Triton X-100) through a polytetrafluoroethylene membrane.
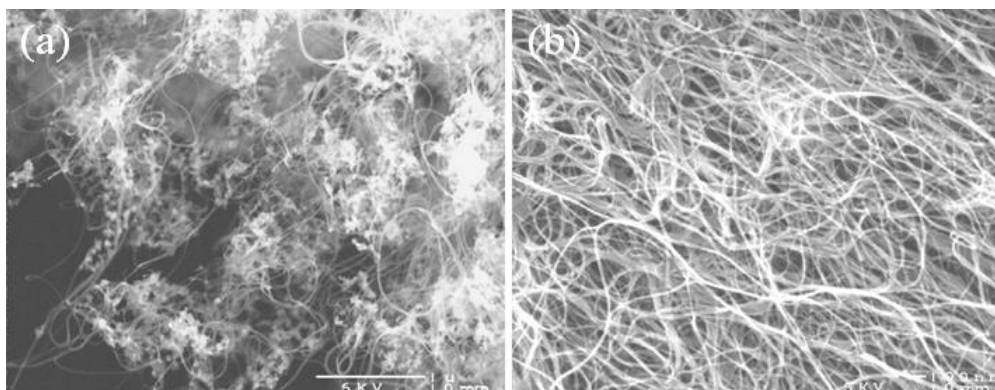
Figure 8. Electron micrographs of (a) raw bundles of nanotubes (SWCNTs) and (b) purified buckypaper [122].

Muramatsu et al. [123] made thin, flexible, and tough buckypaper by filtering a stable solution of double-walled CNTs (DWCNTs)/ethanol. After nitrogen absorption studies, the authors found the pore size in DWCNT paper was three times greater than that in SWCNT paper. TGA results also showed an enhancement of ~200 ºC in oxidation resistance due to the coaxial structure of DWCNTs. Li et al. [124] correlated the mechanical and electrical properties of buckypapers to the nanotube structure after synthesizing MWCNTs on catalysts with different Mo/Co ratio. Buckypaper made of nanotubes synthesized with a catalyst ratio of 1.5 showed strength and electrical conductivity values of 15 MPa and 61 S/cm. With tubes grown at Mo/Co ratio higher than 1.5, the papers turned out to be too brittle to be tested. This suggested that the integrity of buckypapers got compromised by a higher proportion of structural defects within the nanotubes.

By macroscopically manipulating an array of CNTs, grown by CVD, Wang et al. [12] innovated the preparation of nanotube-based buckypaper through a process called "domino pushing." This method produces thin films by continuously compressing–much like domino-toppling–an array of vertically aligned nanotubes (Figure 9). The high degree of tube alignment and flexibility achieved through this method produced electrical and thermal conductivity values

in the range of 2×10^4 S/m and 153 W/(m K). While showing better performance in electrical and thermal conductance, the paper's specific capacitance relative to mats with randomly oriented nanoparticles (87.5 F/g) dropped to 81 F/g as a consequence of less surface area available for charge storage.
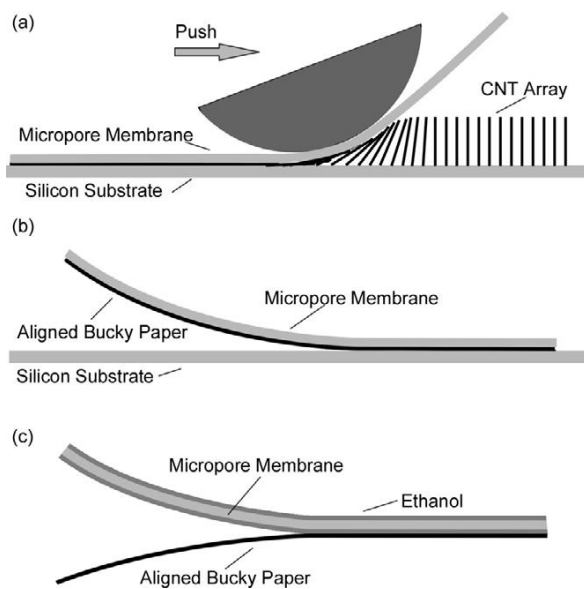
Figure 9. Domino pushing approach [12]: (a) forming aligned CNT paper, (b) peeling the paper off the silicon substrate, (c) peeling paper off the porous membrane.

Unlike traditional mixing methods (sonication, shear mixing, etc.), nanoparticle-based thin films (buckypaper) are an effective route to create composites with high nanoparticle content. Yet, the fabrication of composites with highly entangled nanoparticle network requires multiple stages with a wide-range of characteristics. Through techniques resembling the processing of conventional fiber-reinforced polymers, buckypapers can be laid up to form composites with high nanofiller volume fraction. Wang et al. [4] produced buckypaper-based composites after fabricating SWCNT papers through a filtration approach, infiltrating diluted epoxy along their thickness direction, and curing them using a hot press. When compared to the neat composite, the storage modulus for the final composites increased by 349-492% with a nanotube loading of up to

39%. Further microscopic examinations revealed that the epoxy saturated the SWCNT papers effectively despite their low permeability. Gou et al. [125] used the well-known vacuum-assisted resin transfer molding (VARTM) process to laminate CNF paper and glass fibers together. The porous CNF papers, comprising highly entangled nanofibers and short glass fibers, were placed in the middle or at the surface of laminates. As a result of energy dissipation within the CNF paper, the damping ratios at high frequency increased by 200-700% with minimum variation in the nanocomposite tensile strength.
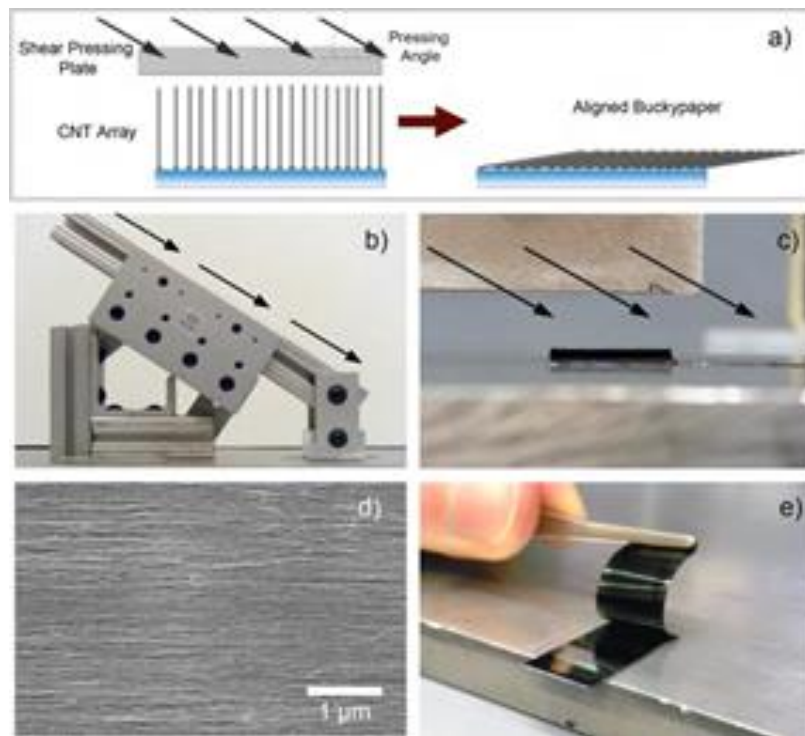
Figure 10. Shear pressing of CNT array [126]: (a) CNT array morphology before and after shear pressing; (b) shear pressing tool; (c) close up of the parallel plate before pressing the array; (d) electron micrograph of preform showing the alignment of CNTs; (e) removal of aligned CNT preform from substrate before resin infusion.

In a different effort, Bradford et al. [126] pioneered a shear pressing approach to convert an array of vertically aligned CNTs into a thin sheet of horizontally aligned tubes (Figure 10). To form nanocomposites, the aligned CNT sheets were immersed in a diluted solution of epoxy and

then cured at elevated temperature. The resulting parts showed a substantial improvement in mechanical and electrical properties. At a CNT volume fraction of 27%, based on TGA data, the nanocomposites exhibited tensile strength, elastic modulus, and electrical conductivity of 402 MPa, 22.3 GPa, and 77 S/m, respectively. These results were superior to those obtained for nanocomposites with randomly oriented CNT sheets.

Later, Liu et al. [127] attempted an alternative approach to fabricate composites with aligned CNT sheets. The process involved the direct winding of a vertically aligned CNT array onto a rotating mandrel that is being sprayed with a diluted solution of polyvinyl alcohol (PVA). Figure 11 shows the schematic of the process. The width and thickness of unidirectionally-aligned CNT composites were controlled by varying the mandrel size, and curing was performed between two hot plates. By outperforming the properties of other polymers, the nanocomposites exhibited tensile strength, toughness, and electrical conductivity of 1.8 GPa, 100 J/g, and 780 S/cm with a tube fraction of 65 wt%, correspondingly.
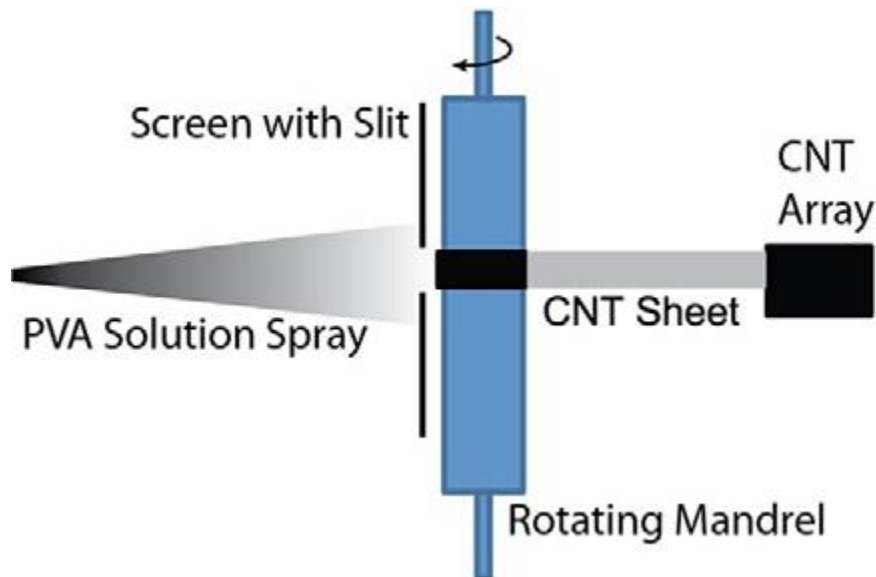
Figure 11. Schematic of spray winding process [127]. Nanotubes are continuously pulled onto a rotating mandrel while a diluted PVA solution is deposited.

Besides the inherent challenge of managing thin films with thickness in the micron range, the composite fabrication by shear pressing or direct pulling has other shortcomings such as high impurity content in nanoparticles, film coupling with substrate, lack of control over lateral dimensions, and low matrix permeability. Thus, new approaches are essential to develop the new generation of advance materials.

CHAPTER 3

SYNTHESIS OF CARBON NANOFIBER THIN FILMS

3.1. Materials

Pyrograph III PR-24-XT-PS CNFs were used to fabricate the nano-engineered thin films. These CNFs have a diameter ranging from 60 nm to 150 nm and a length of more than 100 μm. As provided by Applied Science Inc., the estimated iron content is less than 14000 ppm and the calculated surface area is 42 m^2/g. Based on these data, the CNFs close the dimensional gap between carbon nanotubes (diameters of 1-80 nm) and their predecessor carbon fibers (diameters of 5-10 μm). Figure 12 despites the unique structure of CNFs, commonly referred to as cup-stacked carbon nanotubes.
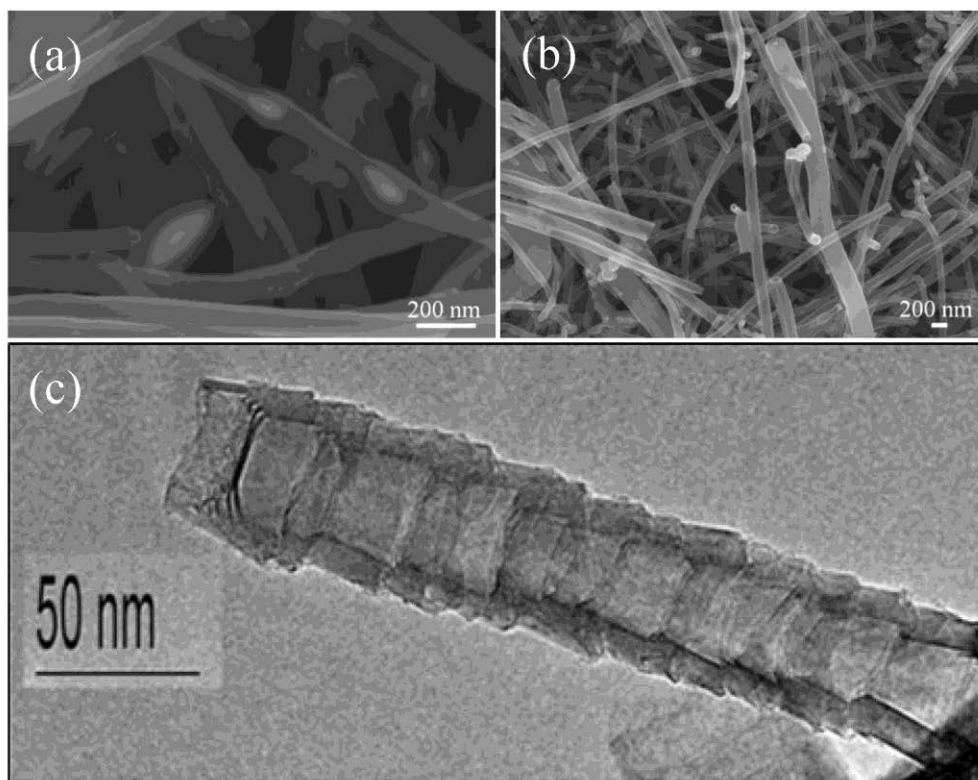
Figure 12. (a, b) SEM images of as-received CNFs and (c) TEM image indicating their unique cup-stacked structure [128].

A solvent-free dispersing agent (surfactant BYK-191) was obtained from BYK additives and instruments. Its composition is based on a copolymer solution with pigment affinic groups (acid and amine) and its density is 1.07 g/ml. All other chemicals were obtained from Fisher Scientific and used as-received.

3.2.   Functionalization of Carbon Nanofibers

The effective fabrication of nano-engineered thin films entails the formation of a well-dispersed colloidal suspension. Often, two routes are used to accomplish this: 1) the non-covalent and 2) the covalent functionalization. The non-covalent functionalization involves the use of surfactant to coat the as-received CNFs and repel their strong van der Waals forces. This leads to nanoparticle stabilization in a medium that can later be used to make a thin film. The covalent functionalization, on the other hand, comprises the structural modification of as-received CNFs. The CNFs are functionalized to the extent of having surface charges, which permit their stabilization in an aqueous medium by overcoming the attractive forces in the absence of surfactant. This practice, nonetheless, requires a careful balance between refluxing time and temperature in order to graft moieties on the CNFs' surface without compromising their structure or properties significantly, as reported in previous investigations [88].

The carbon oxidation reaction is one of the most used methods involving elemental carbon. Because of its simplicity, this reaction is the key to altering the physicochemical properties of carbon such as wettability and solubility. Thus, it serves as a building block for tailoring the specific surface of carbon-based materials. In this study, the as-received CNFs were functionalized through an oxidation reaction carried out using a liquid-phase oxidizing agent–nitric acid (HNO_3)– as outlined elsewhere [129] and shown in Figure 13. Oxidation by this reagent introduces foreign elements (carboxylic acid, carbonyl, hydroxyl, etc.) onto the carbonaceous surface and alters the

intrinsic structure of the pristine material by increasing its surface area. Essentially, to obtain carboxylic acid-functionalized CNFs, 2.5 g of as received CNFs (AR-CNFs) were mixed with nitric acid (500 ml) in a round bottom flask and cup-horn sonicated in a water bath for 20 minutes at amplitude of 170 W. Subsequently, the mixture was refluxed for two hours at boiling point under continues stirring. After the time elapsed, the blend was diluted in 2000 ml of water, vacuum filtered using a nylon membrane of 0.45 μm pore size, and rinsed with ultrapure water and acetone until chemically neutral. The oxidized nanofibers, herein referred to as OCNFs, were dried overnight inside an oven set to 100 ºC, hand-ground, and stored in a desiccant box until further use.
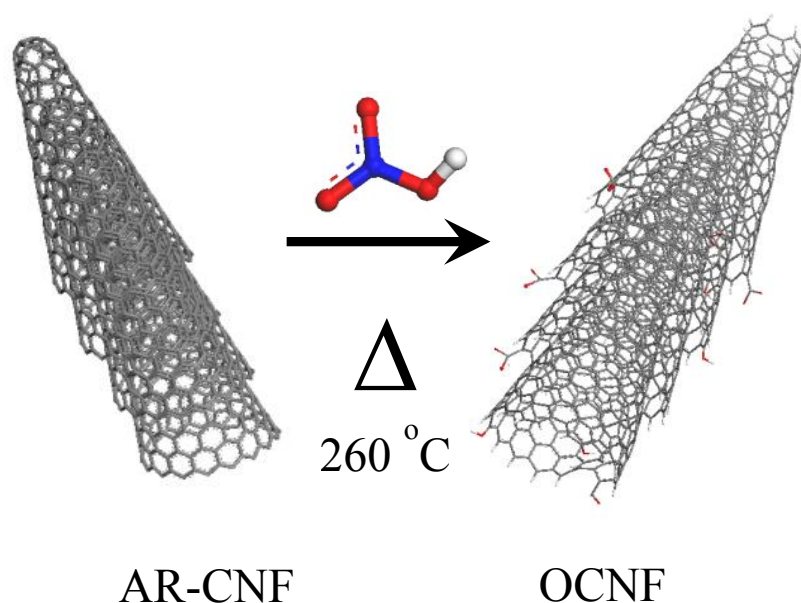

Figure 13. Oxidation scheme for carbon nanofibers.

3.3.   Fabrication of Nano-engineered Thin Films

In this study, two types of nanofibers –AR-CNFs and OCNFs– are utilized to fabricate thin films. As above-mentioned, the OCNFs were chemically treated for two hours in order to cause less structural damage and preserve their maximum length. Unlike the OCNFs, the AR-CNFs were

non-covalently modified with surfactant; a chemical reagent often used to stabilize and uniformly disperse particles in a liquid medium. For this, a surfactant solution (1.25 ml) was first diluted with acetone, hand-stirred, and sonicated for 10 minutes to achieve a homogenous mixture. Thereafter, a separate mixture of AR-CNF/acetone (250 mg/450 mL) was tip-sonicated in a water bath for 30 minutes. Immediately after 10 minutes of sonication, the surfactant/acetone solution was added to the AR-CNF/acetone mixture and sonicated for the remaining time (20 minutes) to obtain the AR-CNF/surfactant/acetone solution.

Two types of non-rolled CNF thin films were made before mechanical compression through a rolling process: non-rolled surfactant-treated AR-CNF (NR-SCNF) and non-rolled OCNF (NR-OCNF) films. To prepare NR-SCNF, the CNF/surfactant/acetone solution was filtered through a 0.45 μm pore size nylon membrane and continuously rinsed with excess acetone to remove trapped surfactant. The preparation of the NR-OCNF followed a similar process. A colloidal suspension was prepared by bath sonicating 250 mg of OCNFs in 900 ml of ultrapure water for one hour. The resulting suspension was then filtered through a nylon membrane. Both NR-SCNF and NR-OCNF films were obtained by peeling them off from the membranes after drying for one hour in a convection oven set to 100°C.

A novel processing approach was utilized to fabricate dense CNF thin films. During this process, both NR-SCNF and NR-OCNF were mechanically compressed by applying shear force with a three-roll-mill. Each thin film was placed on the feed roll and rolled at approximately 3 rpm, with each size of the thin film rolled for 10 times per gap size (defined as the separation between two rolls). Note that only two out of the three rolls in the calendering machine were used to perform the rolling process. To fabricate rolled OCNF films, three layers of NR-OCNF were rolled at gap size of 90 μm, 60 μm, and 30 μm and they were referred to as R-OCNF-90, R-OCNF-

35

60, and R-OCNF-30, respectively. Each NR-OCNF film was rolled from 120 μm to the desired gap size with a 20 μm reduction during gap adjustment, except for R-OCNF-90 and R-OCNF-30 films, in which the gap size was decreased by 10 μm upon reaching 100 μm and 40 μm, respectively. It was experimentally found that NR-OCNF would crack when rolled at gap size below 30 μm following the above-mentioned procedure.

To produce a rolled surfactant-treated AR-CNF film (R-SCNF), a layer of NR-SCNF was rolled from a gap size of 120 μm to 100 μm. Rolling it at a gap size below 100 μm would cause distortion and fragmentation of the thin film. Note that NR-SCNF and R-SCNF films were prepared and used as a basis of comparison in this research. Figure 14 illustrates the schematic for the fabrication of dense CNF thin films.
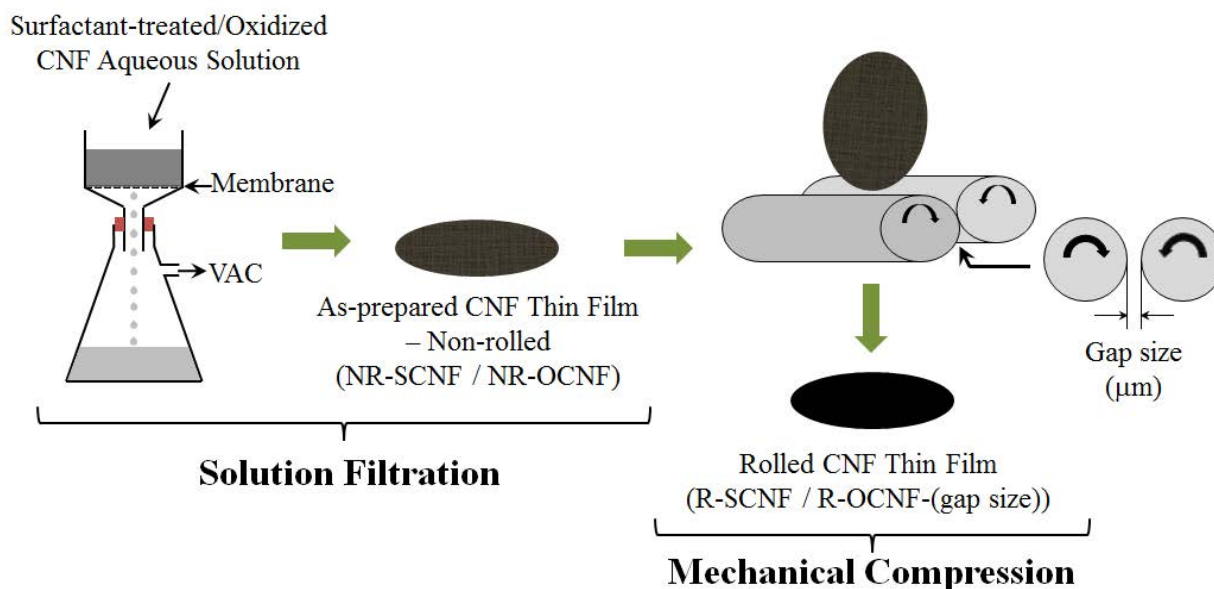

Figure 14. Schematic for preparing non-rolled and rolled CNF thin films.

3.4. Nanofiber Characterization

The chemical modification of CNFs was investigated by fourier-transform infrared spectroscopy (FTIR) and thermo-gravimetric analysis (TGA). FTIR is a powerful analytical

technique used to identify mostly organic functional groups (bonds) in any material. In principle, a compound is irradiated with infrared radiation using a high frequency laser beam. The absorbed infrared radiation excites molecules into an elevated vibrational state. The resulting energy emitted by the sample–measured in wavelength (cm^{-1})–characterizes its molecular structure. In this work, FTIR spectra were acquired using an attenuated total reflectance (ATR) accessory, which permits direct examination of solids without complex sample preparation. Each sample consisting of ~2 mg of CNFs was encapsulated between the ATR crystal (germanium) and the ATR tower to obtain the spectrum. IR spectra were recorded from 400 cm^{-1} to 4000 cm^{-1}.

TGA, on the other hand, is a thermal analysis technique commonly used to evaluate materials that exhibit mass loss or gain due to oxidation, moisture, and decomposition. In this method, the material property changes are measured relative to temperature increase; hence, the results (e.g. percentage of weight change) are normally plotted as a function of temperature. For the sample preparation, ~5 mg of CNFs were weighed and put in a high-temperature platinum pan. The pan was placed inside the TGA furnace, and the test was run from 45 °C to 500 °C in nitrogen atmosphere at a temperature ramp rate of 10 °C/min.

3.5. Characterization Methods of Nano-engineered Thin Films

All CNF thin films were tested for tensile strength using a testing stage equipped with a 20 N load cell and 1 mN resolution (Linkam TST 350). Four dog-bone shaped specimens were cut from each thin film with a die, as specified in ASTM D1708. Tensile coupons were gripped and tested in displacement control at a rate of 5 μm/s while force (N), displacement (mm), strength (MPa), and strain (%) were concurrently recorded. A test was considered valid if failure occurred within the gage section. Figure 15 depicts the tensile coupon configuration and testing stage.
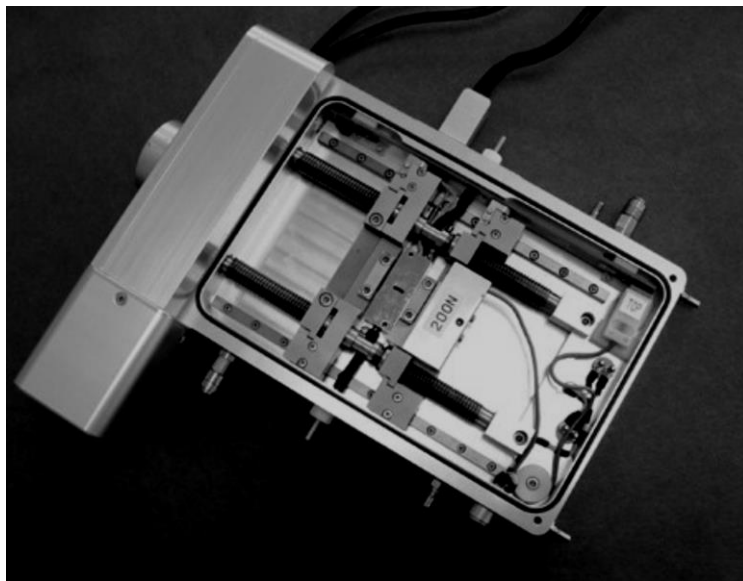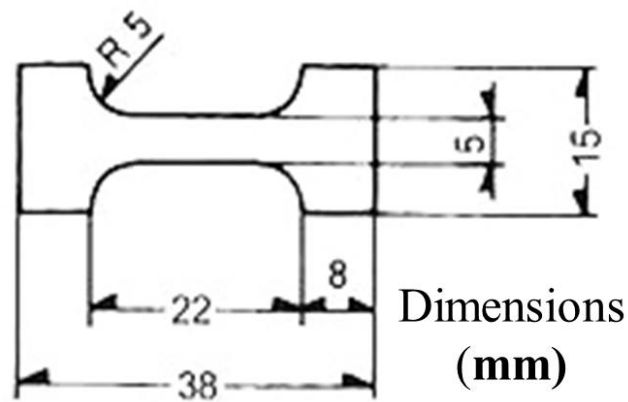
Figure 15. Specimen configuration and tensile testing stage [130].

Electrical conductivity was determined by a four-terminal sensing (four-point-probe) method. In contrast to the two-terminal sensing approach, this technique uses two pairs of current-carrying and voltage-sensing electrodes to make accurate measurements. The separation of current and voltage electrodes reduces the impedance contribution–common in two-point-probe method–of both wiring and contact resistance, making this measurement technique favorable for thin film applications. To perform this test, three rectangular specimens were cut using a pair of razor blades. The dimensions of the samples were 5 mm x 20 mm. Each specimen was placed in a custom-made electrical test fixture (Figure 16). The two ends of the specimen were held with a pair of aluminum

plates pre-coated with silver paint to ensure good electrical contact. Sample resistance was measured, and the resultant electrical conductivity value was obtained using Ohm's law. Thickness dimensions were estimated with a high precision micrometer and by averaging at least ten measurements per thin films.

To calculate the thin film bulk density, a circular section from each film was cut (ϕ 11.1125 mm or 7/16") and weighed with a microbalance. Density was calculated by dividing the thin film's weight by its corresponding volume.
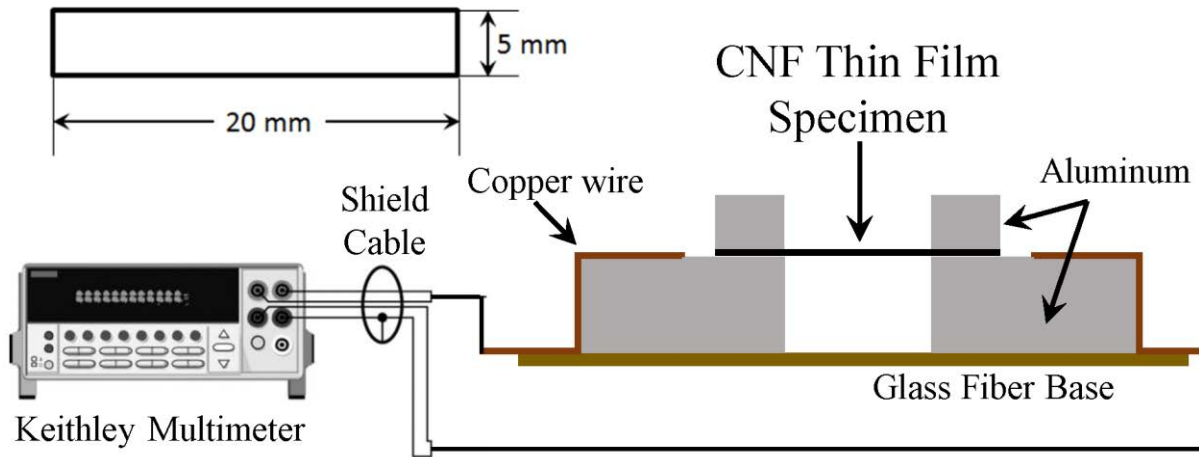
Figure 16. Specimen dimensions and four-point-probe testing fixture. Electrical resistance was measured using a Keithley multimeter [131].

CHAPTER 4

RESULTS AND DISCUSSION

4.1. Characterization of Functionalized Carbon Nanofibers

4.1.1. Fourier-transform Infrared Spectroscopy

Infrared (IR) spectra were recorded in the absorbance mode to confirm the presence of functional groups on the surface of carbon nanofibers. Figure 17 depicts IR spectra for as-received and oxidized carbon nanofibers (AR-CNFs and OCNFs). As expected, AR-CNF shows a featureless spectrum (Figure 17a) distinctive of carbon with no organic moieties grafted on its surface. In the absence of elements that can be excited by infrared radiation, the IR band tends to be absorbed by the compound and shows a line along the frequency range, as shown in the figure. By contrast, the spectrum for OCNF (Figure 17b) depicts peaks confirming the presence of carboxylic acid (-COOH) groups on the nanoparticle's surface. Absorption bands at 1707 cm^{-1}, 1201 cm^{-1} and 2956 cm^{-1} correspond to the atomic vibration frequencies of carbonyl (C=O), carbon-oxygen single bond (C-O), and hydroxyl (O-H) compounds that form part of COOH groups, respectively [132, 133].
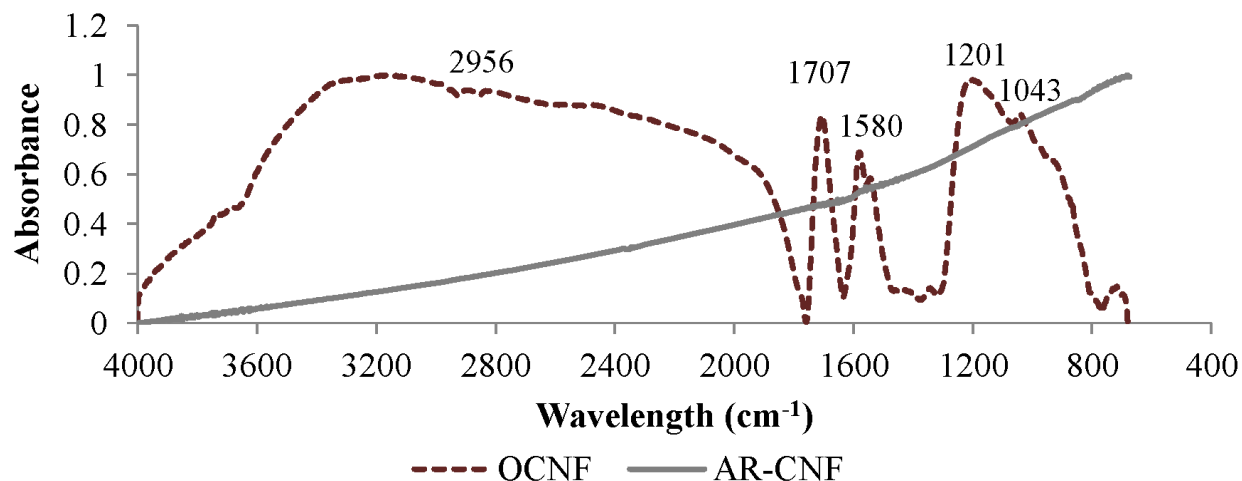
Figure 17. FTIR spectra of as-received (AR-CNFs) and oxidized carbon nanofibers (OCNFs).

4.1.2. Thermo-gravimetric Analysis

TGA was performed to further validate the presence of carboxylic acid groups on CNFs after treatment with nitric acid. Plots of mass change against temperature are shown in Figure 18. The analysis of AR-CNFs shows an insignificant weight loss over the entire temperature range, characteristic of untreated nanofibers. OCNFs, on the other hand, present a substantial amount of mass change over the same temperature range. To better identify the transitions of mass change with temperature, derivative TG curves were recorded and are also shown in the same figure. An initial weight loss from room temperature to ~130°C represents water desorption (evaporation) from nanoparticles as a result of temperature increase. Close to 220 ºC, another inflection point is observed with a total weight loss of 8% from 150 ºC to 380 ºC. According to previous reports, this temperature range describes the detachment of carboxylic acid groups from carbon when heated in an inert atmosphere [134].
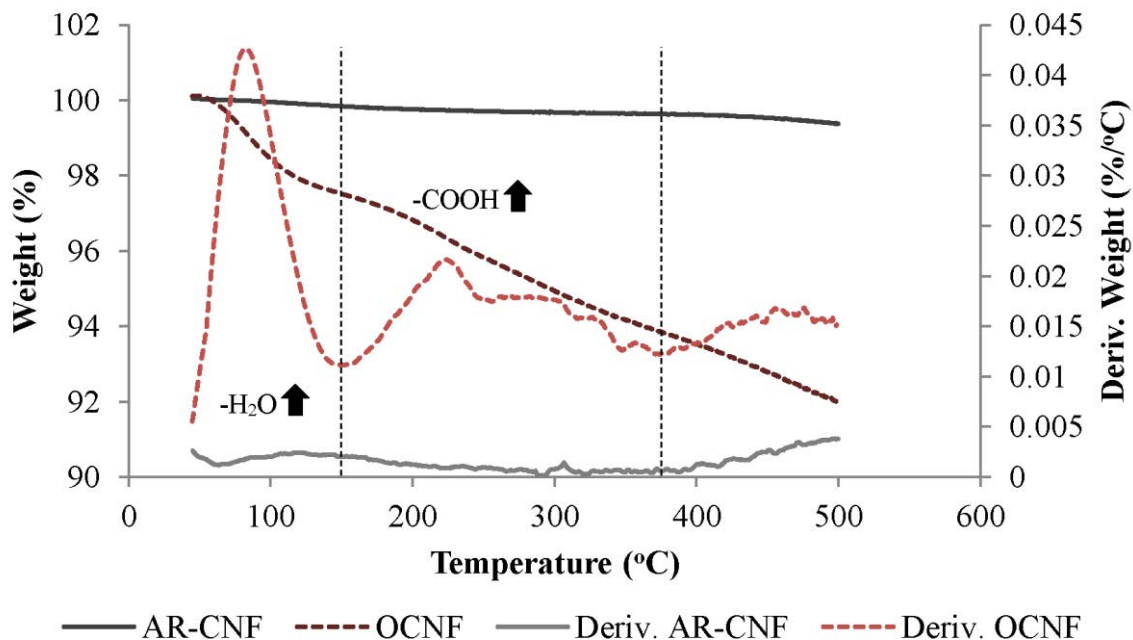
Figure 18. TGA plots for as-received CNFs (AR-CNFs) and oxidized CNFs (OCNFs). Dash lines represent the derivative TG curves.

41

While carboxylic acid is the main functional group derived from the liquid oxidation method used in this work, there are by-products formed during functionalization that at low concentrations are not detected or distinguished by FTIR. These are mostly related to carbonyl, phenol, anhydrite, and lactone compounds. Because of overlapping bands in the IR spectrum, the precise recognition of each compound is challenging by FTIR. Nevertheless, TGA can give indications on whether compounds other than carboxylic acid exist on the nanofibers' surfaces. Closely inspecting Figure 18, the OCNF plot shows continuous degradation after 400 $^{\circ}$C. This indicates the presence of by-products as a result of nitric acid treatment [134]. Over time, however, a plateau value should appear with further heating due to complete removal of organic groups.

4.1.3. Scanning Electron Microscopy

Because of the aggressive conditions in which AR-CNFs need to be exposed to change their inert structure with reactive species such as carboxylic acid, it is imperative to assure that the treatment performed herein does not destroy the unique conformation of nanofibers by creating amorphous carbons. Figure 19 illustrates the effect of oxidation on the CNFs' morphology.

Microscopic examinations reveal that the cup-stacked morphology of nanofibers is still preserved after chemical oxidation, noted by the fibrous structure of individual OCNFs in Figure 19c. Notice that a rough morphology appears at the edge of the nanofiber cone, as pointed in Figure 19b. This may be the result of structural rearrangement due to grafting of organic moieties. It also indicates a reduction in fiber length because of the harsh treatment conditions. Further inspection at high magnification shows surface roughness on the nanofiber wall (Figure 19d), which is a clear indication of sidewall functionalization. This is encouraging because it allows better interaction between nanofibers in close proximity or between nanofibers and matrix in composite materials.

42
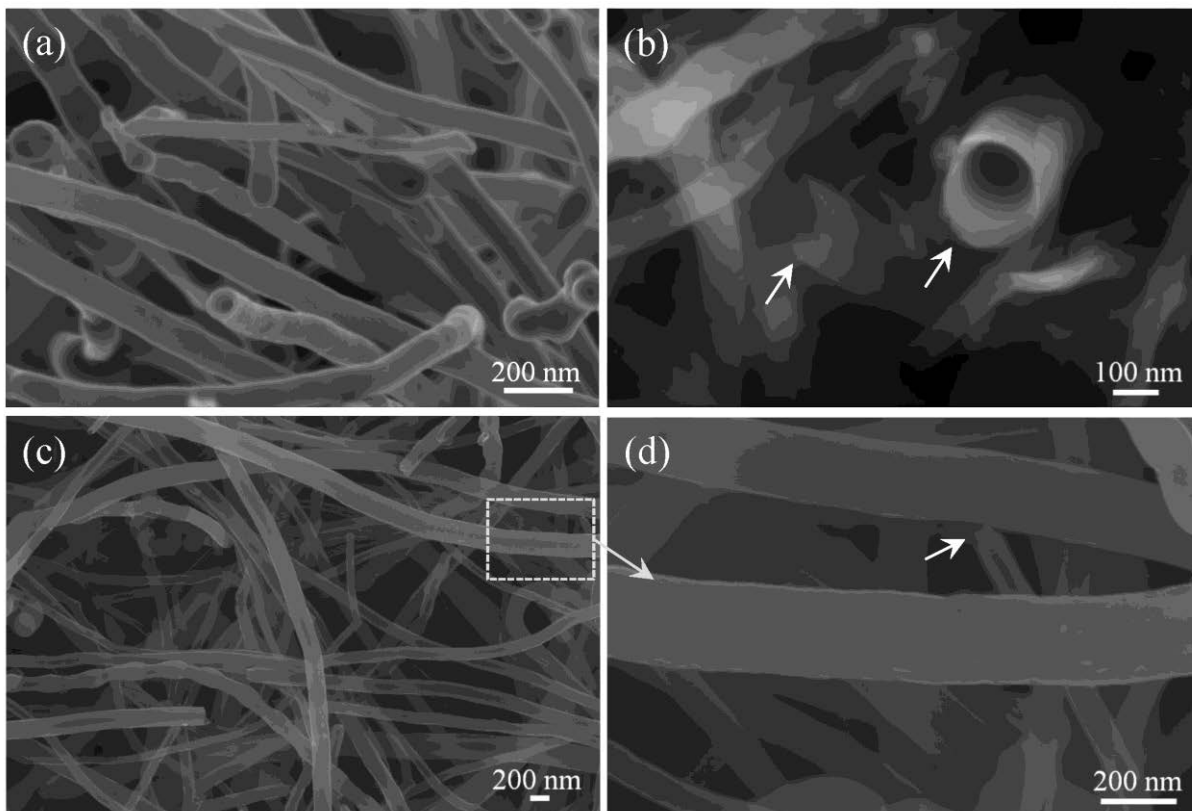
Figure 19. Scanning electron micrographs of carbon nanofibers: (a) as-received CNFs (AR-CNFs); (b) roughness around the cone of oxidized CNFs (OCNFs); (c, d) surface imperfections on the outer layer and the tip of OCNFs.

While exposure of AR-CNFs to nitric acid results in the fragmentation of long fibers into short ones (based on SEM images), it is not clear from FTIR or TGA if catalyst particles remain on the nanofibers' surfaces. Therefore, another type of analysis is needed to characterize the CNF composition. Figure 20 illustrates the elemental analysis for CNF before and after chemical oxidation. Qualitative measurements by Energy-dispersive X-ray Spectroscopy (EDS) show the complete removal of iron (Fe) catalyst and silicon (Si) substrate after oxidization treatment. As expected, the X-ray emissions for OCNF depicts peaks associated with carbon (C) and oxygen (O) only.
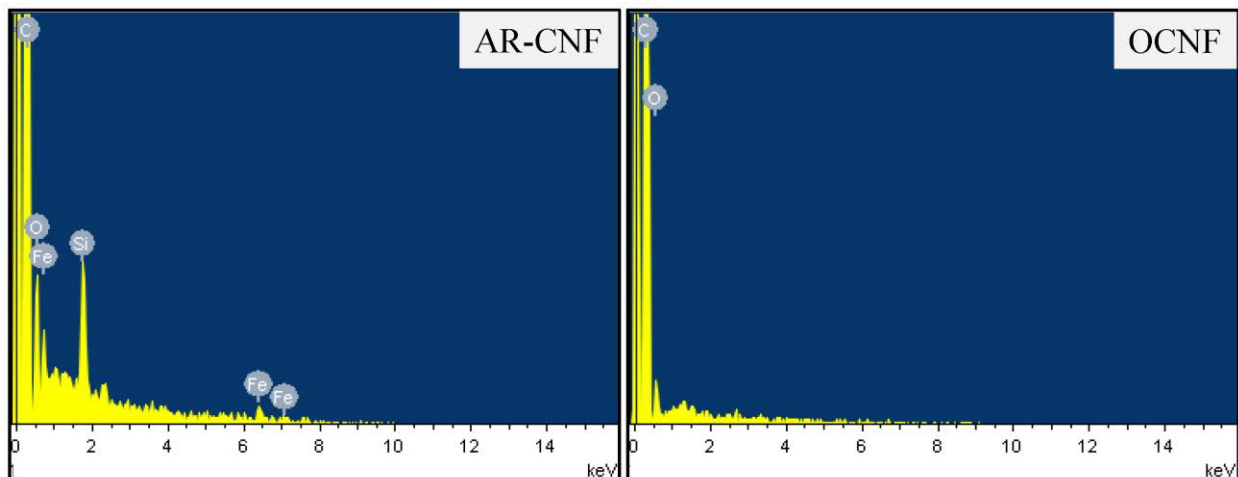
Figure 20. Energy-dispersive X-ray spectra for as-received CNF (AR-CNF) and oxidized CNF (OCNF).

Based on these results, the oxidation procedure performed in this study can successfully introduce carboxylic acid groups onto the CNF's surface without compromising its integrity. Moreover, it opens new avenues to functionalize nanofibers with other organic species by means of condensation reactions with carboxylic acid –amine, alcohol, etc.

4.2. Thin Film Morphology

Figure 21 shows optical images describing the surface morphology of both non-rolled and rolled SCNF thin films. Before mechanical compression, the nanofibers in the NR-SCNF film are loosely stacked on top of each other, and the surface morphology appears to be highly porous, as observed in Figure 21a. Quite the opposite is noticed in Figure 21b. The nanofibers in the R-SCNF film seem to displace and form small bundles of closely interconnected fibers due to the rolling process. Inspection at higher magnification (images 2b) shows that these bundles are highly entangled and possibly creating an interlocking mechanism, which might promote superior electrical and mechanical properties. In addition, it appears that the amount of free space decreases after rolling the film, which makes perfect sense since the film density increases as the fibers

approach to each other. Hence, further reduction in inter-filler junctions may be expected as the rolled thin film surface morphology becomes denser with the rolling process.
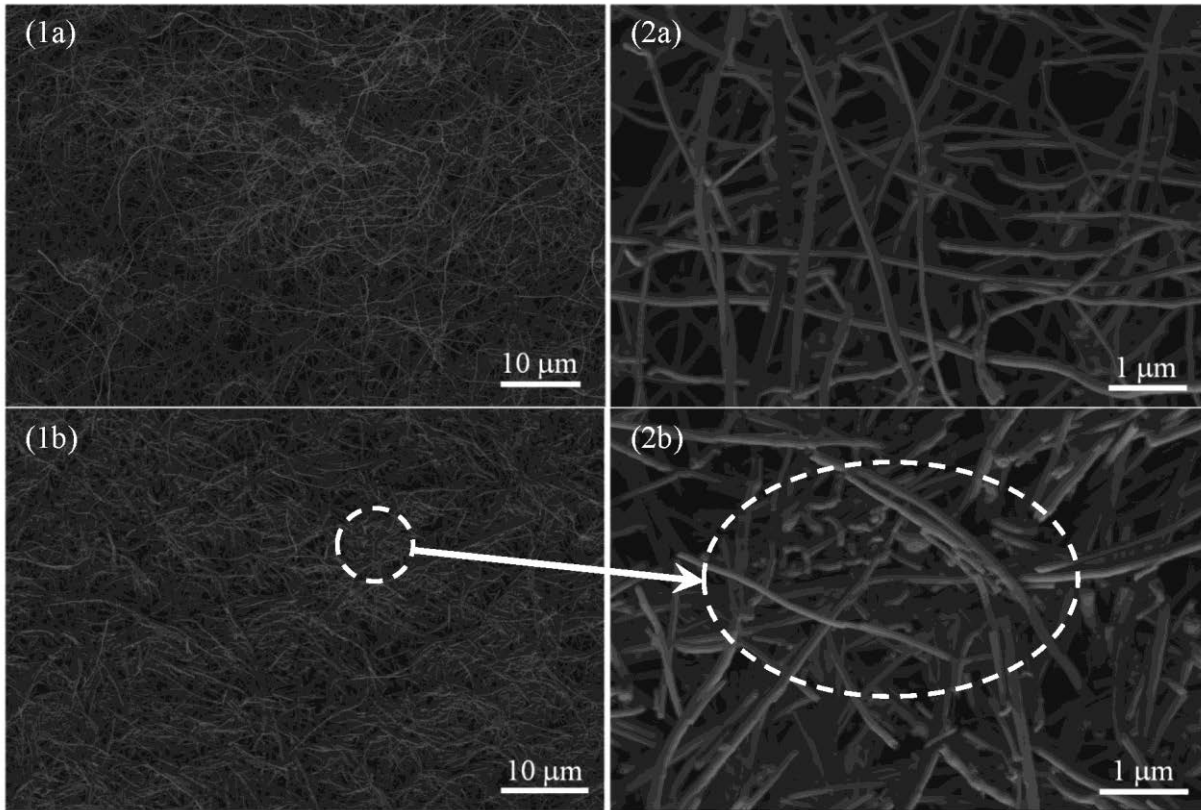
Figure 21. Surface morphology of thin films fabricated with surfactant treated CNFs. (a) displays a thin film before rolling (NR-SCNF) and (b) shows a thin film after rolling (R-SCNF).

There is an indistinguishable difference between the two non-rolled thin films (NR-SCNF and NR-OCNF) after comparing their surface morphology (Figure 21a and Figure 22a). Like in the case of NR-SCNF film, the morphology of NR-OCNF comprises a highly porous entangled fiber network. The OCNFs seem to be loose, and there is little fiber-fiber contact. Conversely, there is a distinct change in surface morphology of non-rolled OCNF films as a result of the rolling process at different gap sizes. As indicated in Figure 22b, patches of CNFs form throughout the film's surface after rolling a NR-OCNF film at a gap size of 90 μm. The nature of the solution filtration method creates thickness irregularities which are continuously compacted as the film

passes between rolls. As such, film sections with thickness higher than 90 μm are being displaced and compressed first to create a film with a much more uniform thickness distribution. Moreover, there are sections in the film within which there is no direct contact between fibers, suggesting that there is still space for fiber movement.

Further film compaction by rolling at 60 μm causes a reduction in interstitial space between fibers (Figure 22c). The CNF patches seem to separate with further compression, and small pinholes appear on the OCNF film due to nanofiber displacement. Apart from the pinholes, there is uniformity of nanofibers throughout the film, which becomes important for generating higher electron transfer rates.

After rolling at a gap size of 30 μm, the thin film shows uniformity throughout its surface (Figure 22d). The pinholes observed after rolling at 60 μm seem to close completely, which suggests that the film has reached its maximum packing density. In other words, rolling at gap size below 30 μm will cause fragmentation of the film since there is not more free space for the nanofibers to move through during compression, as found experimentally.

At high magnification (image 2d), the OCNFs appear to be highly interconnected with each other, forming a dense entangled fiber network. An increase in fiber-fiber contact intensifies the interatomic interactions–van der Waals forces or secondary bonding–between nanofibers. Therefore, high fiber interactions may result in thin film with superior properties.
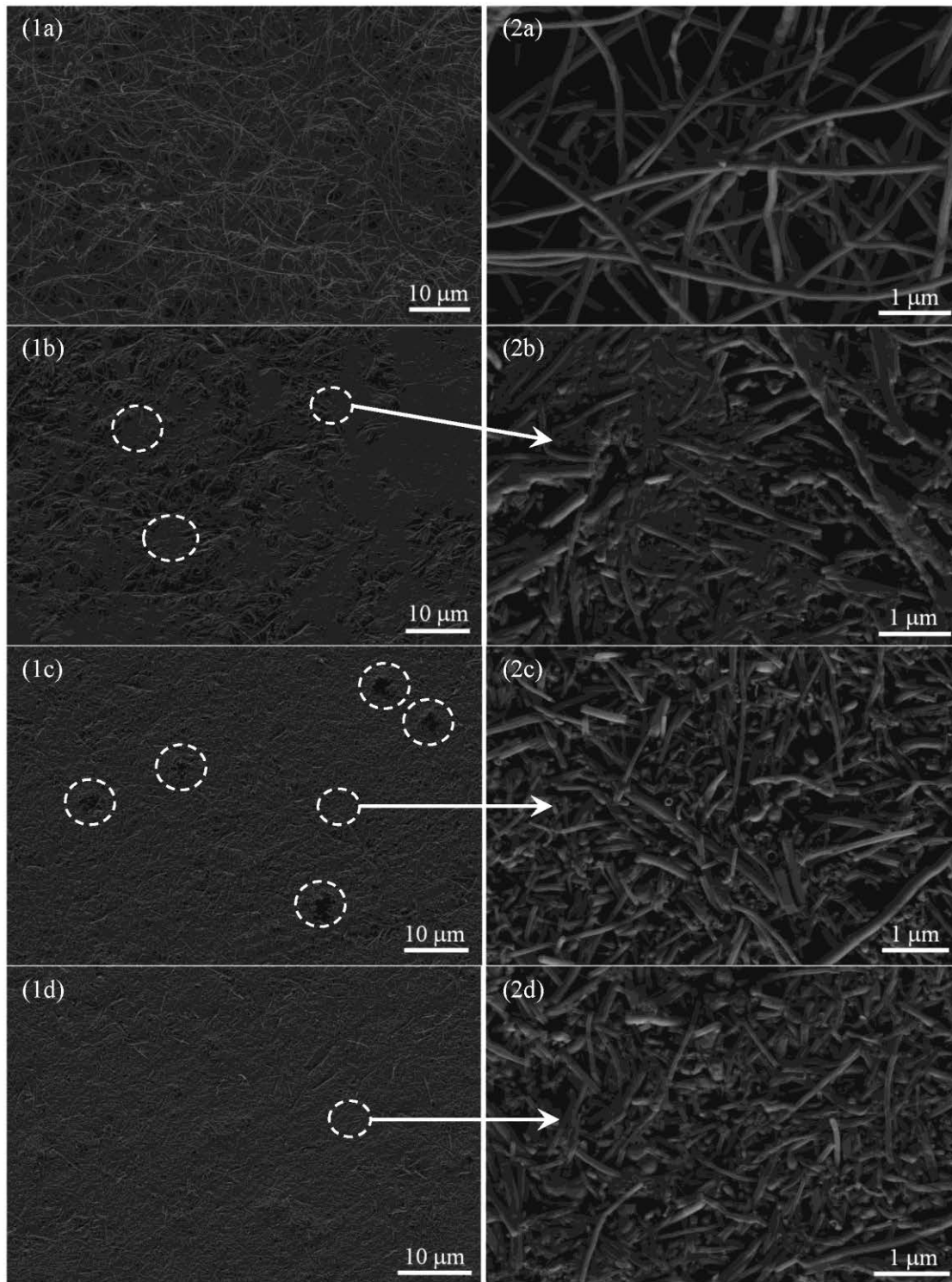
Figure 22. Surface morphology of thin films fabricated with carboxylic acid functionalized CNFs (OCNFs). (a) displays a thin film before rolling (NR-OCNF) and (b, c, d) show thin films after rolling at gap sizes of 90 μm, 60 μm, and 30 μm (R-OCNF-90, R-OCNF-60, and R-OCNF-30), respectively.

To analyze the effect of mechanical compression (rolling process) on physical properties of CNF thin films, the average thickness and bulk density are calculated and presented in Table 2. Before rolling, the NR-OCNF film has an average thickness of ~175 μm with a standard deviation of ±12 μm. There is a progressive decrease in thickness for all rolled OCNF thin films, which is consistent with the increase in packing density observed in Figure 22. Because of lower interstitial space between nanofibers, the thickness of NR-OCNF reduces to a value of 65 μm after being rolled at a gap size of 30 μm. Notice that a constant standard deviation of ±3 μm is achieved due to the rolling process. This indicates that the rolled OCNF films have a much more uniform thickness distribution than the NR-OCNF. It also agrees with the microscopic images presented in Figure 22. Thin film morphological changes cause rearrangement and compaction of nanoparticles.

TABLE 2

AVERAGE THICKNESS AND BULK DENSITY OF CNF THIN FILMS

Sample Name	Process	Thickness [StDev] (μm)	Bulk Density (g/cm³)
NR-SCNF	Non-rolled, surfactant treated CNF	356 [±18]	0.150
R-SCNF	Rolled, surfactant treated CNF	173 [±9]	0.247
NR-OCNF	Non-rolled, oxidized CNF	175 [±12]	0.280
R-OCNF-90	Rolled at 90 μm, oxidized CNF	102 [±3]	0.431
R-OCNF-60	Rolled at 60 μm, oxidized CNF	79 [±3]	0.583
R-OCNF-30	Rolled at 30 μm, oxidized CNF	65 [±3]	0.681

Because of marginal experimental variation in weight and area between OCNF thin films, it is presumed that the change in thin film thickness represents the pivotal parameter for the change in bulk density. In other words, plotting density with respect to thickness (Figure 23) and comparing the bulk density of non-rolled and rolled OCNF thin films, it is clear that density

increases linearly (R^2 of 0.9083) with thickness reduction. However, the thickness-density relationship can be better fitted if high precision instruments are utilized to measure the film thickness and more experimental data are included in the regression model. Based on these results, it is believed that both mechanical and electrical properties of rolled thin films can enhance by reducing the interstices between particles in the highly entangled CNF network.
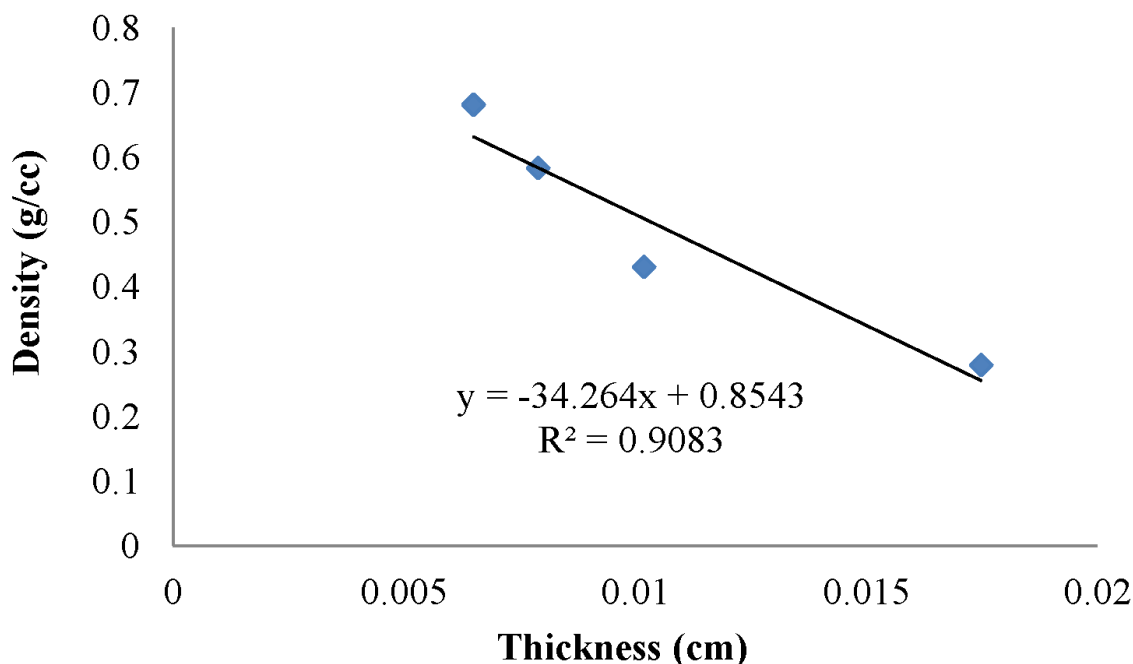
Figure 23. Change in bulk density with respect to thickness variation for OCNF thin films. Linear regression model expresses the relationship between thickness (x) and density (y) [135].

4.3. Mechanical and Electrical Characterization of Thin Films

Figure 24 shows representative tensile strength-strain curves for the thin films fabricated with AR-CNFs and OCNFs. The NR-SCNF film exhibits the lowest ultimate strength (0.33 MPa) and the highest strain to failure. These strength and strain values may be caused by: 1) weak interaction between particles because of surfactant treatment, which lowers van der Waals forces; 2) low level of nanofiber entanglement, as corroborated by the density value in Table 2 and observed in Figure 21. A modest increase in strength to 1.5 MPa is noticed after fabricating a thin

film with acid-functionalized CNFs (NR-OCNF film). Such improvement in strength seems to be associated with a gain in density (Table 2), which at the same time increases the nanofiber-nanofiber contact as well as their van der Waals interactions. Besides van der Waals forces, to some extent it is likely that the high strength of OCNF thin film is related to the electrostatic dipole-dipole interaction between carboxylic acid molecules present on the nanofibers' surfaces. Because of their polarity, carboxylic acid groups can engage in energetically favorable hydrogen bonding by creating partial covalent bonds (dimers) between hydrogen bond acceptor (hydroxyl) and hydrogen bond donor (carbonyl) groups [136]. These bonds are in general stronger than van der Waals interactions, but weaker than ionic bonds (covalent bonds). Thus, the high strength of the NR-OCNF film may be the result of enhanced nanofiber-nanofiber interaction due to hydrogen (H) bond formation. This observation seems to be in line with the results found by other authors, in which H-bonding between nanotubes with COOH moieties promoted their assembly into thin films [137, 138]. A schematic is shown in Figure 25 describing the possible H-bond interaction between OCNFs.
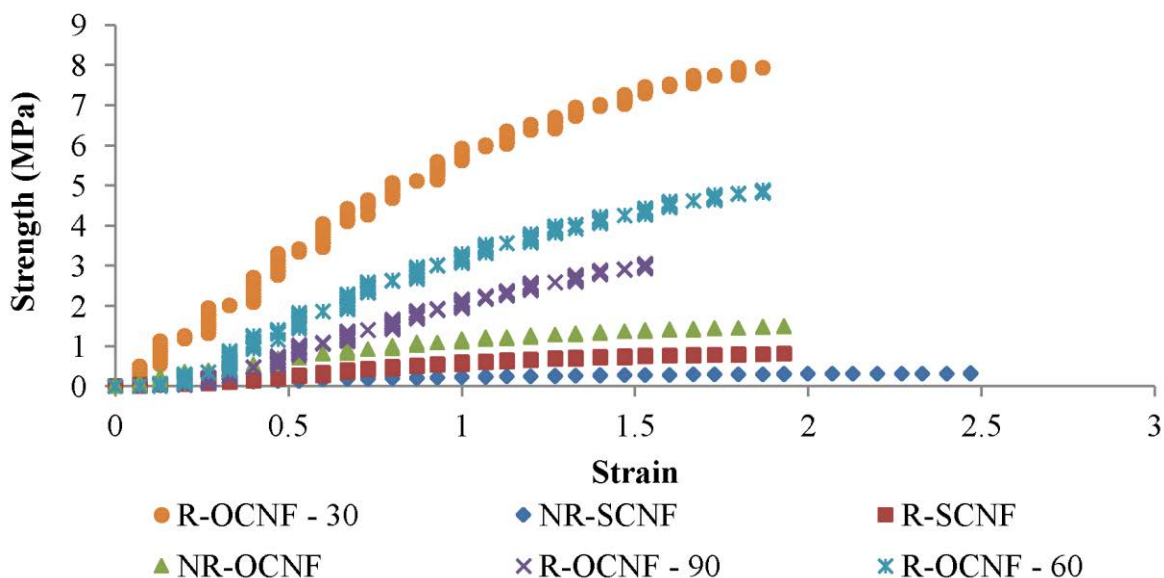
Figure 24. Representative stress-strain curves for the CNF thin films.
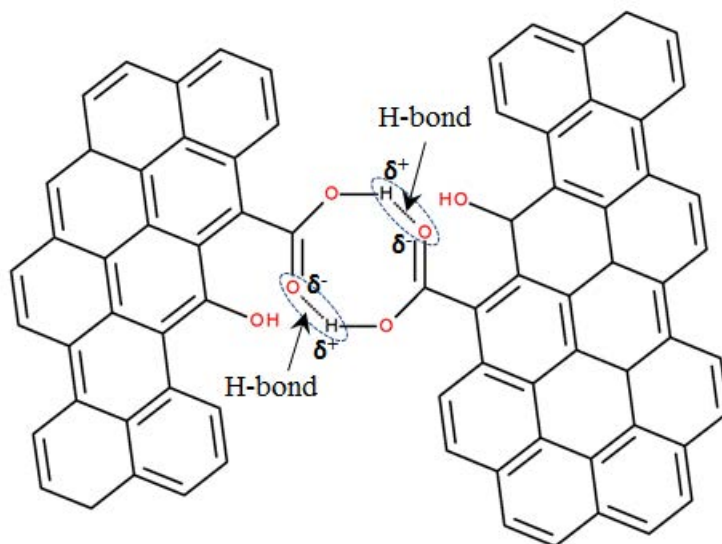
Figure 25. Formation of hydrogen (H) bonds between carboxylic acid moieties on oxidized nanofibers. H-bond between partial positive H atom and lone pairs on partial negative oxygen (O) atom.

Even though chemical functionalization has been shown to be detrimental to the individual properties of CNFs [139], it appears that for the cases of thin films, it not only permits fabrication of free-standing films without the need for polymer solutions, but also creates films with superior properties. As observed in Figure 24, the ultimate tensile strength for the thin film fabricated with surfactant-treated CNFs increases because of the rolling process (R-SCNF) but its value (0.81 MPa) is lower than the one obtained for NR-OCNF film (1.5 MPa). This result suggests that the non-ionic nature of surfactant, although being useful for stabilizing particle in a medium, hinders the interaction between nanofibers in the films by reducing their van der Waals forces. Thus, this low particle-particle interaction results in low-performance thin films.

One good way to support the aforementioned statement is through TGA. By measuring mass change with respect to temperature, it identifies whether any trace of surfactant remains in the thin film after the fabrication process. Tests performed in nitrogen atmosphere at 10 $^\circ$C/min ramp rate are depicted in Figure 26. While the OCNF thin films show mass losses characteristic

51

of moisture evaporation and carboxylic acid detachment, both SCNF films exhibit inflection points after ~300 °C due to decomposition of surfactant. Therefore, the minimized interatomic interactions between particles due to residual surfactant on the nanofibers' surfaces result in thin films with low strength, as shown in Figure 24.
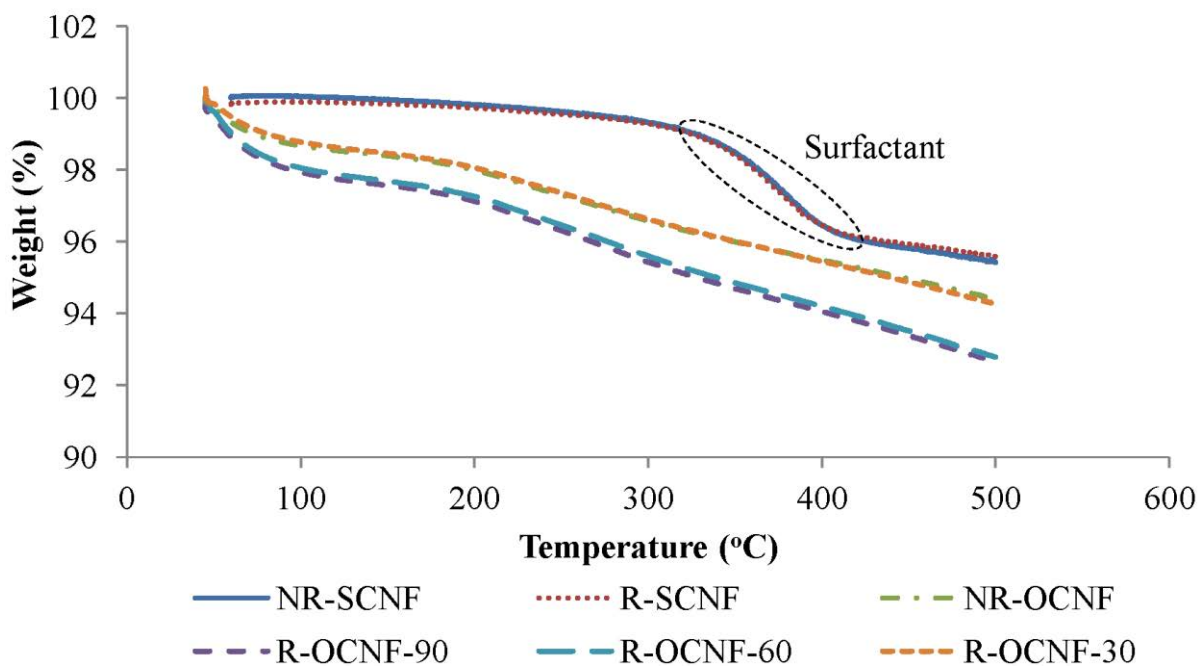
Figure 26. TGA for non-rolled and rolled CNF thin films.

The effect of rolling, on the other hand, becomes evident by the significant boost in strength observed in Figure 24. The film tensile strength consistently increases as a result of mechanic compression at various gap sizes between rolls (e.g. 100 μm, 90 μm, etc.). Rolling the NR-OCNF film at a gap size of 90 μm, 60 μm, and 30 μm increases the tensile strength to 3.05 MPa, 4.88 MPa, and 7.94 MPa, respectively. These results, in fact, are clear indications that higher properties are possible provided that a good nanofiber-nanofiber interaction is achieved.

A different overview of the properties of CNF thin films is presented in Figure 27 and Figure 28. These two figures summarize the values of tensile strength and electrical conductivity for all films fabricated. For films of the same material, both strength and conductivity of rolled

films are in overall superiority to those of non-rolled. It is evident from Figure 27 that the tensile strength of R-OCNF-30 is considerably higher than that of NR-SCNF, indicated by a difference of 1900%. Considering thin films built with OCNFs only, the strength of R-OCNF-30 film is ~390% larger than the NR-OCNF. Likewise, the electrical conductivity of R-OCNF-30 film has a value ~60 times higher than that of NR-SCNF (Figure 28). With respect to OCNF thin films, the electrical conductivity of R-OCNF-30 film increases by ~420% in comparison with NR-OCNF. Overall, these results strongly suggest the use of the rolling process to enhance both tensile strength and electrical conductivity of nano-engineered thin films.
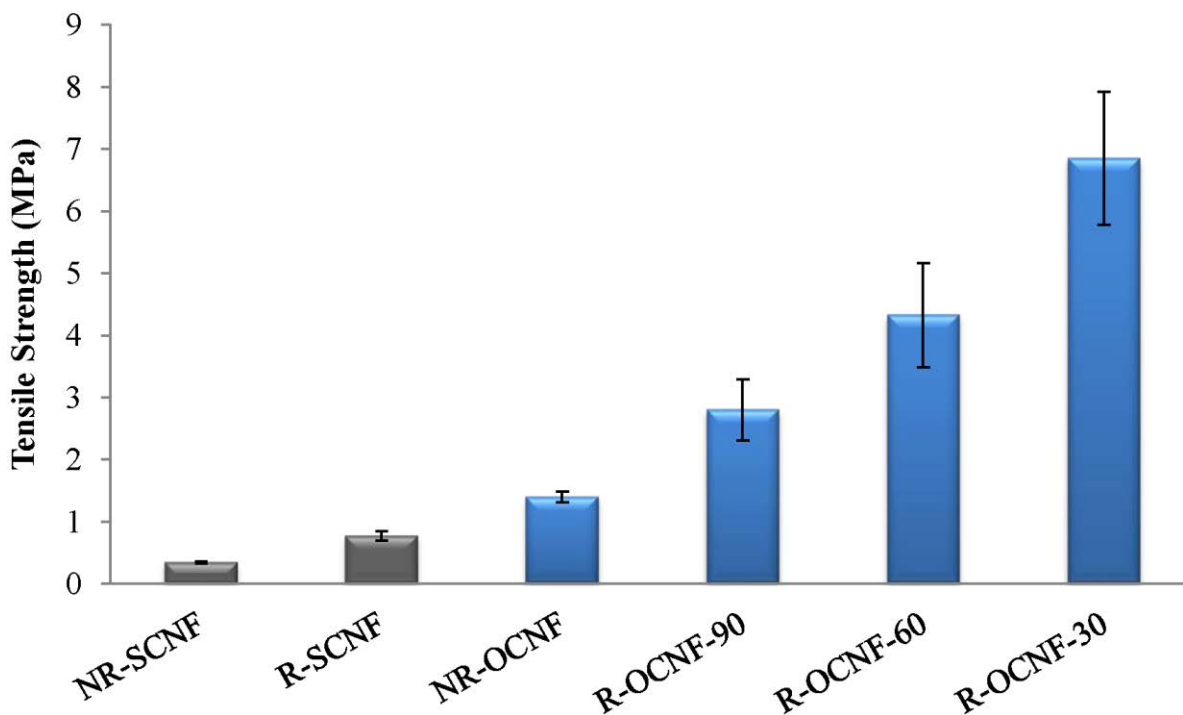
Figure 27. Change in tensile strength of thin films before and after the rolling process [135].

While a uniform thickness distribution can be accomplished by subjecting the CNF thin films to the rolling process, high standard deviations in strength and conductivity arise due to measurement errors in force and resistance. These errors normally amplify as the range of strength and conductivity increases. Based on the trends observed in Figure 27 and Figure 28, thin film

with superior tensile strength and electrical conductivity may be made, provided that the NR-OCNF film is rolled at a gap size lower than 30 μm and its initial thickness remains below 175 μm.
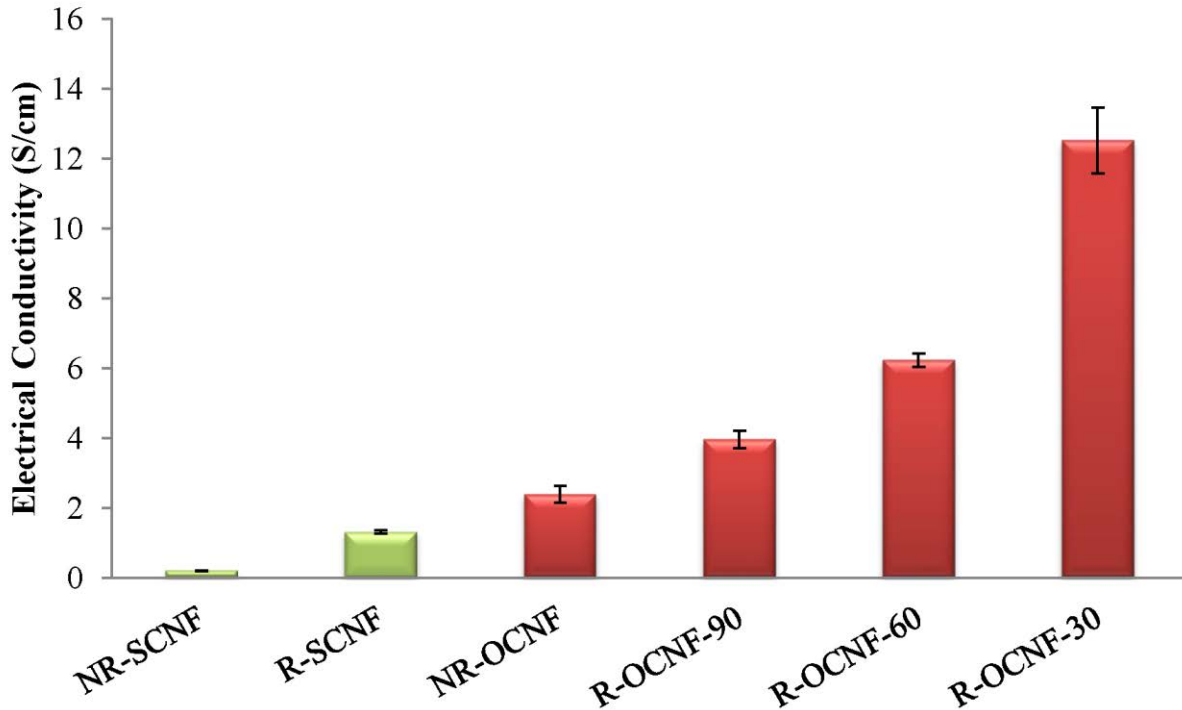
Figure 28. Change in electrical conductivity of thin films before and after the rolling process [135].

The resistance to electric current in powder materials is normally associated with a combination of individual resistances: grain and contact resistance. Thus, particle contact is essential in order to ensure flow of electric charge and measure material conductivity at the bulk level [140]. As reviewed by Euler et al. [141], the conductivity of powders depends on the pressure exerted on them and relates to the elastic-plastic particle deformation. In CNFs, it is valid to assume that the individual conductivity of single particles is high, since they comprise mainly cup-stacked graphene sheets. Nevertheless, the highest contribution to electrical resistance when assembling individual nanofibers in a thin film form is at the interface between nanoparticles [142]. When compressed, the number of electrical contacts augments as a result of the forced proximity of

surrounding nanofibers (Figure 22). Figure 28 demonstrates that, during which the relationship between electrical conductivity and thickness (Table 2) ranges from ~2 S/cm for the NR-OCNF to ~13 S/cm for the R-OCNF-30 film. Without any functionalization post-treatment on the CNFs (SCNFs), the electrical conductivity values for both non-rolled and rolled thin films are below 2 S/cm, which suggests that surfactant shields the nanofiber from electron transfer.

In observing the conductive tendency of thin film built with SCNFs and OCNFs, it is apparent that contact resistance decreases by increasing the packing density between nanofibers through the rolling process. As density changes after chemical oxidization, it seems obvious that the contact resistances are different between thin films fabricated with and without surfactant (NR-SCNF and NR-OCNF), although the film morphologies appear to be alike (Figure 21a and Figure 22a). The oxidation effect on density may therefore be the result of morphology changes, catalyst removal, and incorporation of oxygen compounds, which may explain the density variation between surfactant-based and oxidized CNF thin films. Figure 29 relates the electrical conductivity of OCNF thin films to density. Through a sintering process, Yang et al. [143] altered the bulk density of nanotube-based buckypaper and found a linear relationship between the paper's density and the sintering temperature. Accordingly, the electrical resistivity (the reciprocal of electrical conductivity) of buckypapers showed an exponential tendency as density increased. As previously compared, the bulk density for both non-rolled and rolled OCNF thin films decreases linearly (R^2 = 0.9083) as thickness increases (Figure 23), reaffirming the strong dependency of bulk density on the thin film thickness. With respect to density, on the other hand, the OCNF thin film electrical conductivity increases exponentially ($R^2 = 0.9637$) as observed in Figure 29. This non-linear trend suggests that there are factors other than density affecting the conductive behavior of thin films. It is rather possible that these factors are associated with the fiber-fiber interactions by either van der

Waals attractions or direct contact and measurement error [143]. Even though the thin film fabrication process used in this work differs from Yang's method, the outcomes agree very well with the results presented by the authors.
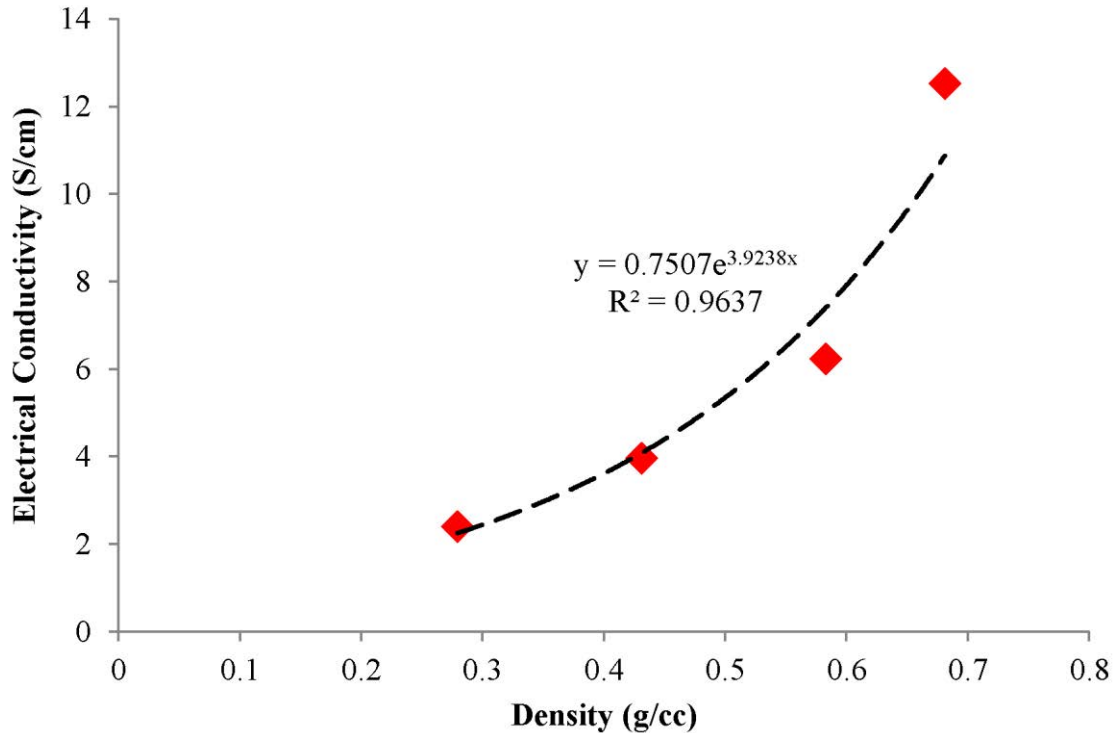
Figure 29. Electrical conductivity with respect to density for various OCNF thin films. Exponential curve fitting equation shows the association between bulk density (x) and electrical conductivity (y) [135].

Of important note is that the statistical models in Figure 23 and Figure 29 allow estimation of bulk density and electrical conductivity of thin film made of any source of nanofibers as long as the fabrication process remains the same.

4.4. Failure Analysis

As observed in the previous section, the rolling process has a positive impact on the thin film properties. Results demonstrate that high inter-filler junctions due to formation of a dense OCNF network enhance both tensile strength and electrical conductivity of thin films (Figure 27 and Figure 28). Based on these findings, it is imperative to examine the fracture surface of both

type of thin films (SCNF- and OCNF-based films) and to analyze whether their failure behavior changes as a consequence of the rolling process. Surface details are presented in the scanning electron micrographs of Figure 30-Figure 33.

After careful examination of the images, several fracture behaviors were identified between non-rolled and rolled thin films. Inspection of Figure 30 reveals a failure mode characterized by nanofiber pull-out, alignment, and network separation for the NR-SCNF film.

Insights into the detachment mechanism during tensile test may be explained from Figure 30a, in which a thin film section is almost torn apart from the network. While the test progresses, it seems that the nanofibers unravel and elongate as the fiber loops are pulled open. This may explain the ductile behavior and high strain failure observed for these specimens in Figure 24. Furthermore, there are no signs of nanofiber damage, perhaps the result of low particle-particle interaction and fiber slippage due to surfactant coating. On different sections of the film, there appear to be nanofiber pull-out and alignment parallel to the loading direction (as pointed by the arrows in Figure 30b) and empty regions similar to voids, hints of low packing density (Figure 30c).
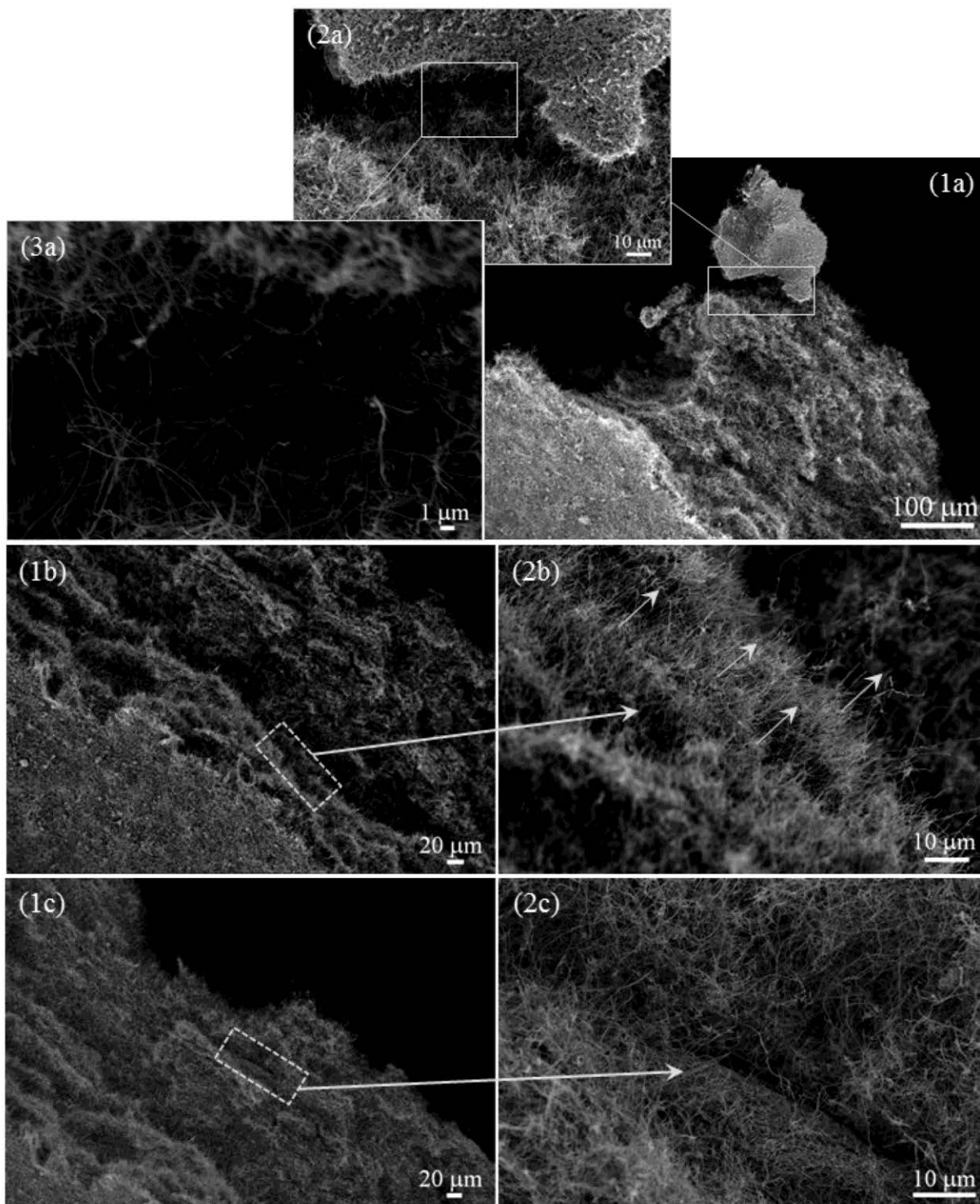
Figure 30. Fracture surface of NR-SCNF thin film.

The R-SCNF thin film presents a rather different fracture behavior. While there are no

significant evidences of nanofiber pull-out, there appears to be fiber alignment due to the applied

tensile force that causes motion of nanofibers toward the loading direction (Figure 31a). There seems to be also a smooth fracture surface across the specimen width (inset of image 1a) as may be expected in a more brittle thin film. As thin film density augments due to mechanical compression, the interactions between nanofibers that come into direct contact with each other increase, intensifying the van der Waals attractions. This phenomenon also creates an interlocking mechanism that allows larger load transfer between fibers to occur when subjecting the film to an external force. As shown by the change in slope of the strength-strain curve in Figure 24, the R-SCNF curve becomes steeper than the NR-SCNF. Hence, the thin film becomes more brittle after rolling.

Looking at a section from which a fragment of thin film separates the network (image 1c of Figure 31), it is clear that, besides being unraveled, the nanofibers in the R-SCNF film are more entangled than those in the NR-SCNF. They seem to detach in bundles rather than individually, as found in image (2b) of Figure 31.

Further examination shows crack formation away from the initial crack plane (Figure 31c), which suggests that there are sections of weak nanofiber interaction. Interestingly, there is another failure mode observed at high magnification. The SCNFs are being fractured during testing, as indicated by the arrows in image 4c of Figure 31. This may be the result of higher interactions and inter-filler junctions between nanofibers. Since the thin film is mechanically compressed due to the rolling process, the van der Waals forces between nanofibers intensify because of higher fiber-fiber contact. Thus, knowing that the nanofiber structure consists of cup-stacked graphitic planes held by van der Waals forces, it is possible that, at certain regions, the contact interactions surpass the forces holding the graphene planes, causing the fiber fragmentation.
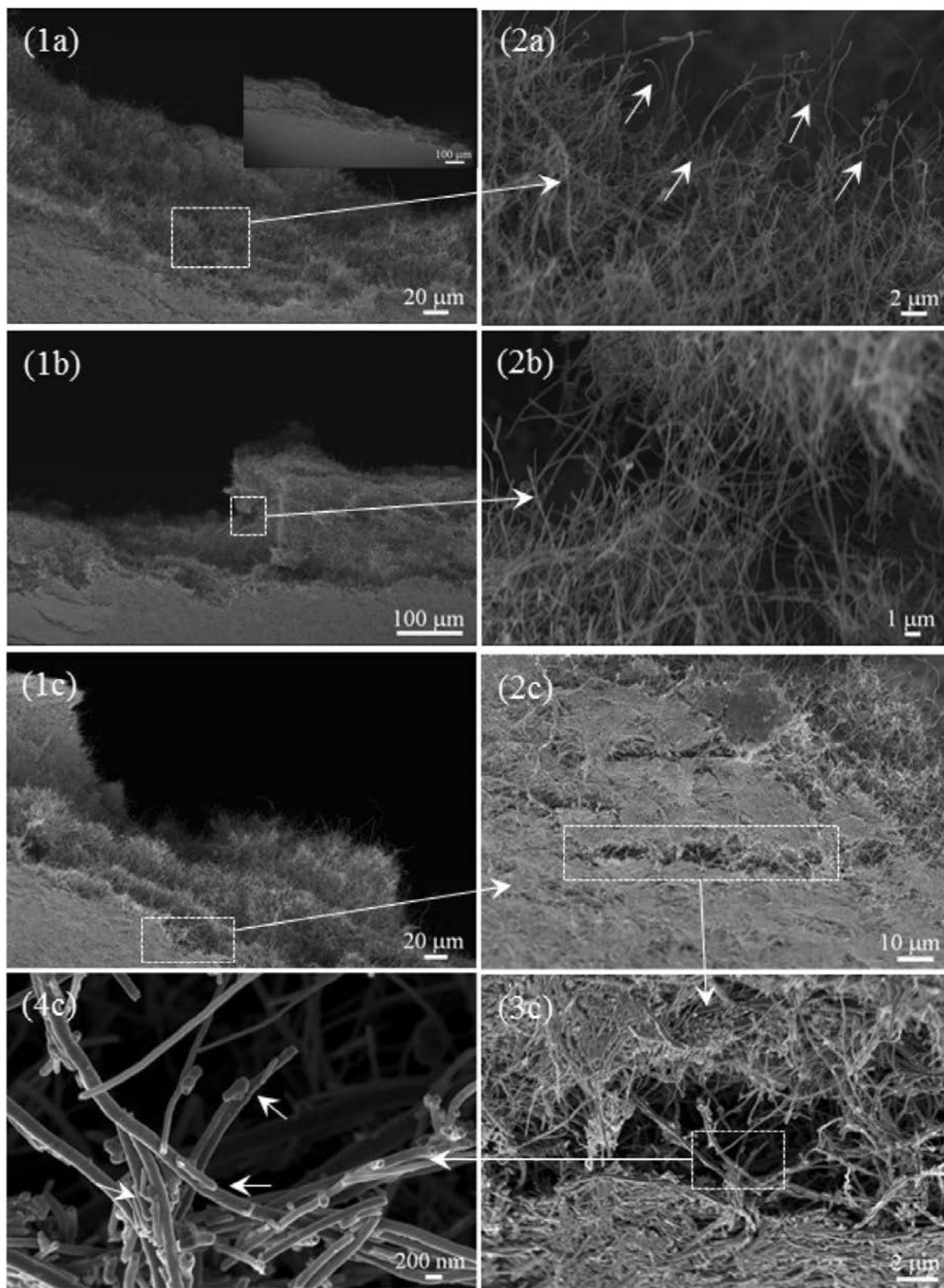
Figure 31. Fracture surface of R-SCNF thin film.

The fracture of the NR-OCNF film, at first glance, shows smooth surface irregularities along the crack plane (Figure 32a). There are also signs of crack growth away from the initial crack plane (inset in Figure 32(1b)), which obviously represents regions of low network interaction and reduced interlocking mechanism between nanofibers.

At magnifications, however, the images reveal other interesting findings. There are sections of free space in which the nanofiber network appears to be loose, possibly originated from fiber sliding (Figure 32(2a)). There is also nanofiber pull-out effect along the edges of the film (Figure 32(1b)), although this effect is not as intense as in the surfactant-treated thin films.

A close look shows that the fiber-fiber interaction seems to be high enough to pull the nanofibers apart. As observed in images 2b and 3b of Figure 32, there is a significant amount of fragmented nanofibers along the free surface. This is a clear indication that the interatomic forces within particles have increased due to acid functionalization. As mentioned previously, the hydroxyl and carbonyl groups of carboxylic acid on OCNFs can produce partial covalent bonds through hydrogen bonding. Being stronger than van der Waals forces, these bonds can overcome the interatomic forces between the graphitic planes of CNFs and thus cause their fragmentation. Further evidences are found by inspecting a nanofiber protruding from the crack plane (Figure 32c). A significant amount of nanofiber fragments is shown to be adhered to the fiber surface. This suggests that the film failure is mainly caused by nanofiber fragmentation rather than network disentanglement, as occurred in NR-SCNF film. It also demonstrates that a greater fiber-fiber interaction is possible by chemically altering the surface morphology of CNFs. These findings agree very well with the tensile strength and electrical conductivity results. The oxidized-based thin film becomes stronger and more conductive than the surfactant-treated thin films.
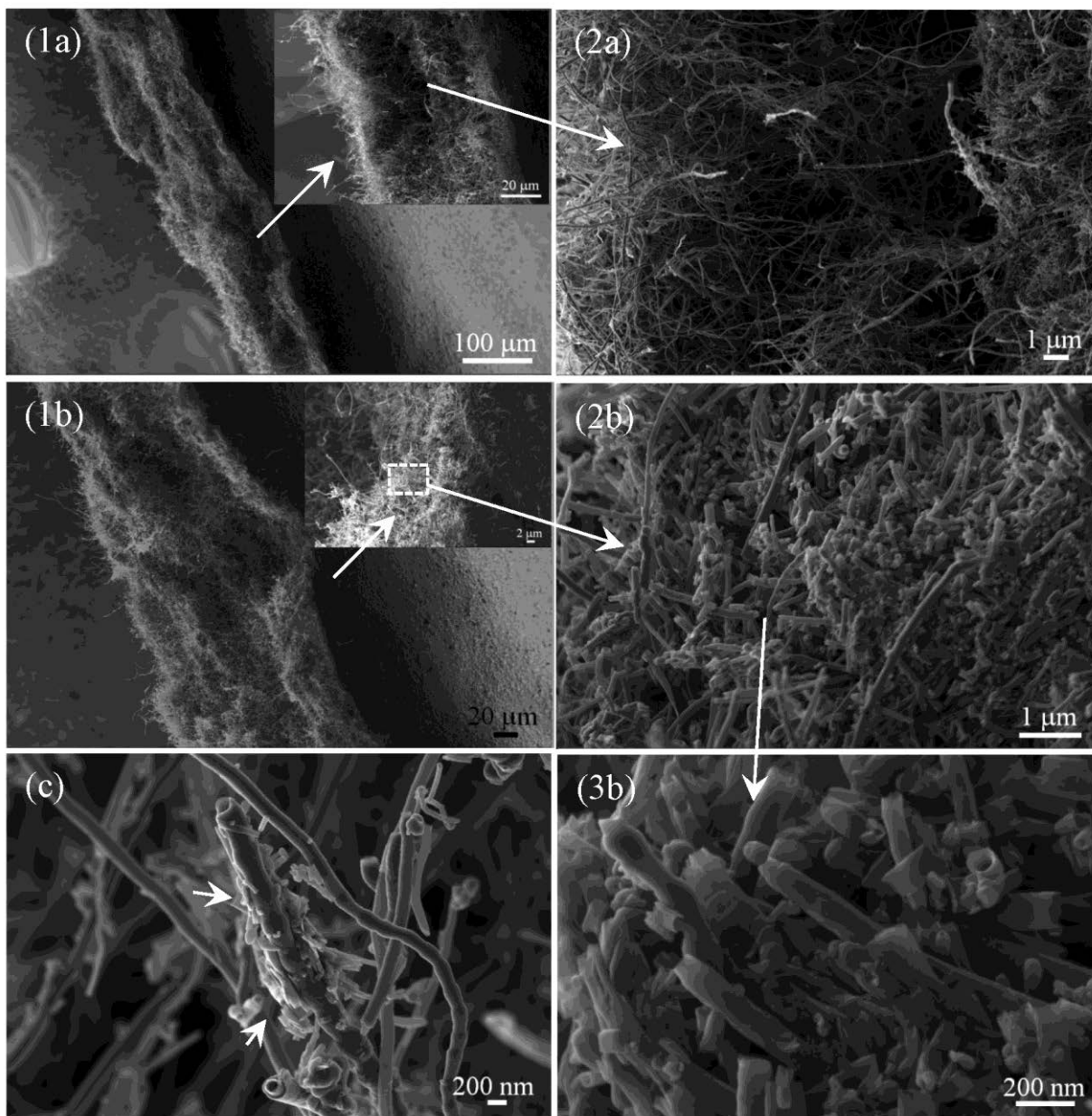
Figure 32. Fracture surface of NR-OCNF thin film.

In contrast to the previous three cases, the R-OCNF-30 thin film shows a failure behavior characteristic of brittle materials (inset of Figure 33a) and consistent with the result shown in Figure 24. Note that the failure mode for R-OCNF-60 and R-OCNF-90 films was similar to R-OCNF-30. As such, their results can be inferred from those discussed below.
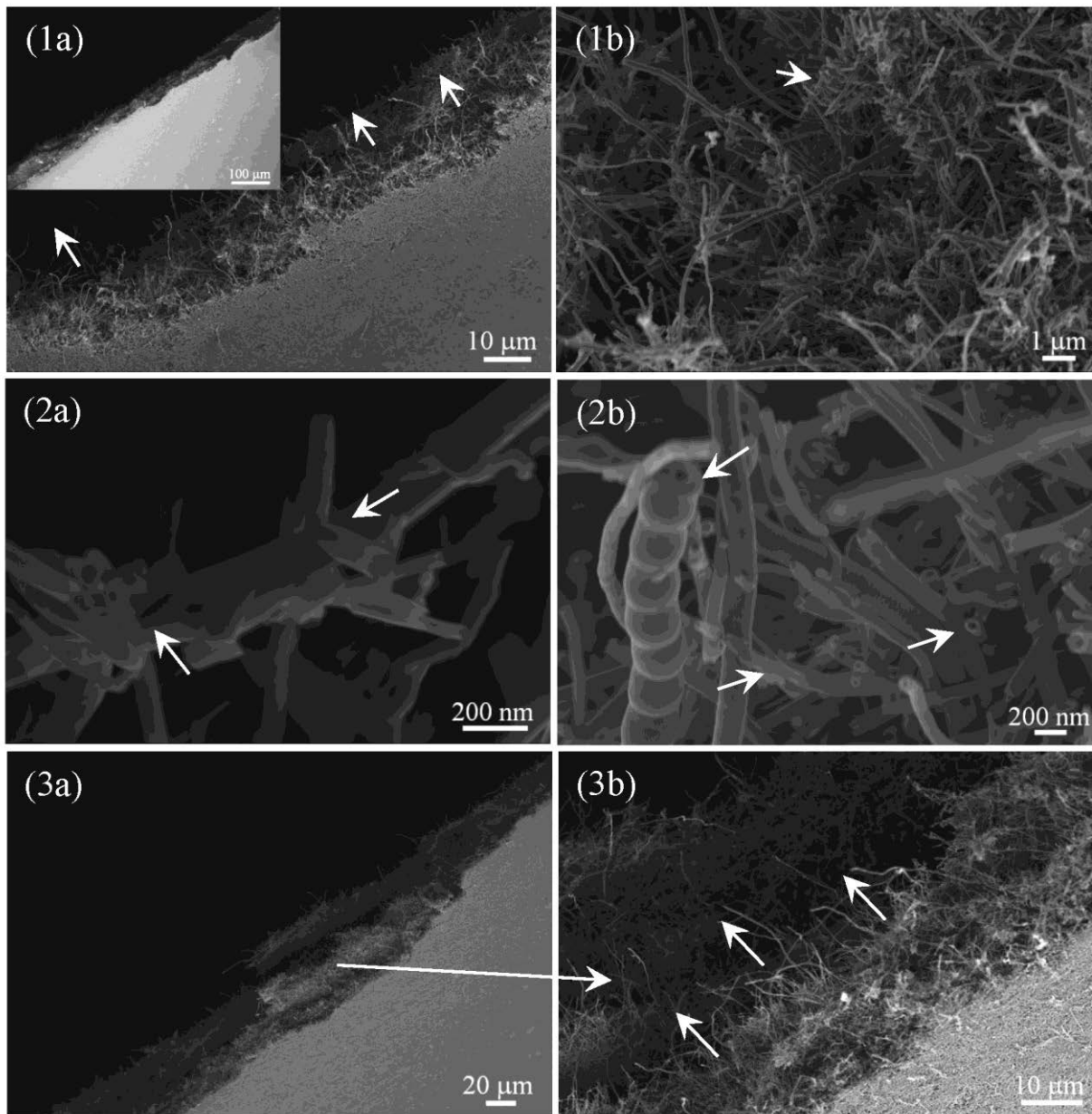
Figure 33. Fracture surface of R-OCNF-30 thin film.

Under the action of an external load, the OCNFs seem to be individually protruding along the specimen's cross section; this is perhaps the result of high interlocking mechanism and pull-out effect within the highly entangled nanofiber network (also indicated by the arrows in Figure 33a).

When imaging at high magnification (Figure 33a/b), there seems to be a significant amount of nanofiber fragments along the crack surface. Like in the NR-OCNF film, the nanofiber's tip gets torn apart as a result of superior fiber-fiber interaction, interlocking mechanism, and possible hydrogen bonding between the carboxylic acid groups on OCNFs. As clearly observed in Figure 33b, the head of some nanofibers fragment and their conical residues remain attached to the wall of other fibers after failure, facts that seem to be common to all OCNF films. These, indeed, validate the strong interatomic interactions between particles. Furthermore, there are sections along the crack plane in which the thin film is not perfectly smooth. An example of this is displayed in Figure 33c. Images reveal a u-shaped fracture across the specimen thickness wherein there is nanofiber alignment parallel to the loading direction (identified by arrows in Figure 33c). Thus, the pull-out effect appears to promote nanofiber alignment as they fracture and slide relative to each other during tensile test, a phenomenon also reported by other authors [144].

CHAPTER 5

CONCLUSIONS

Thin films made of carbon nanoparticles (nanotubes/nanofibers) are a new type of material characterized by a distinct combination of properties, which render them suitable for many applications. While most thin films encompass an entangled network of randomly oriented nanoparticles, their properties are dominated by two phenomena: intermolecular interactions and inter-filler junctions. This work described the processing and characterization of dense nano-engineered thin films fabricated by a novel two-step approach. The process combined solution filtering and mechanical compression to improve interactions and junctions between particles. In the first step, a dilute suspension of surfactant-treated (S) or carboxylic acid-functionalized (O) carbon nanofibers (CNFs) was vacuum filtered onto a filtration membrane to form a thin film. The film, referred to as non-rolled (NR), was obtained after peeling it off from the membrane when completely dry. In the second step, NR-CNF films were subjected to mechanical compression through a rolling process. During this process, the gap or separation between rolls was adjusted to different dimensions–(100, 90, 60, and 30) μm–in order to assess the rolling effect on the film properties.

After inspecting the surface morphology of thin films, electron micrographs revealed significant changes due to the rolling process. The characteristic porous and loosely stacked network structure of NR-(S/O)CNF films changed to a dense and highly entangled network; nanofibers tended to displace and form small bundles of closely interconnected fibers as the film reached its maximum packing density. These findings showed excellent agreement with the corresponding experimental data. The thin film bulk density linearly increased while thickness

decreased as a consequence of the rolling process. Therefore, it is concluded that thickness represents the pivotal parameter for the change in density.

The effect of chemical oxidation became evident when comparing the properties of NR-(S/O)CNF films. The NR-OCNF film exhibited superior properties to the NR-SCNF. This was attributed to improved interaction between OCNFs by either direct contact or secondary bonding (hydrogen bonding) between carboxylic acid molecules, in line with the results reported by other authors. Furthermore, surfactant seemed to hinder interaction and junction between particles by minimizing van der Waals attractions.

Mechanical and electrical test results showed that tensile strength and electrical conductivity were directly correlated to surface morphology. Strength and conductivity increased by 400% when the NR-OCNF film was rolled at a gap size of 30 μm. Based on microscopic observations, this gap size represented the point in which the OCNF film reached its maximum packing density. Hence, greater load and electron transfer were attained as a result of the close proximity between nanofibers.

While thickness and density showed a linear relationship for OCNF films, a different correlation was identified between bulk density and electrical conductivity. The conductivity of OCNF films increased exponentially with increasing density as result of higher fiber-fiber contact. Interestingly, this exponential behavior in conductivity also agreed with the results found by other investigators regardless of the processing techniques used to fabricate nanoparticle-based thin films.

From fracture surface analysis, several failure modes were identified. Non-rolled and rolled SCNF films showed a failure mode characterized by the sequential detachment of nanofiber loops as the films elongate. Based on this, it seems clear that the contact resistance between fibers

decreases due to surfactant, which causes nanofiber slippage and inhibits an interlocking effect. With respect to OCNF films, both types of films portrayed a failure behavior characteristic of brittle materials and consistent with the experimental data. Because of their improved interatomic interactions, the OCNFs fragmented under the action of tensile force. The consistent presence of broken fibers along the crack plane was evidence of an interlocking effect between nanofibers developed due to their change in surface morphology through chemical oxidation. Therefore, it is suggested that the failure of OCNF films is mainly caused by nanofiber fragmentation rather than network disentanglement as occurred in the SCNF films.

The results presented in this study show that the CNF thin film properties can be tailored by adjusting the separation between rolls during the rolling process. The highest properties are achieved when the film reaches its maximum packing density. Based on this, it seems appropriate to state that further improvement in properties can be possible by promoting chemical bonding between CNFs. One route to do this is by performing condensation reactions with carboxylic acid in order to integrate molecules on OCNFs (e.g. amine, coupling agent) that can react with each other.

Manufacturing of thin films from CNFs has potential for future applications. The realization of nano-engineered thin films with optimal properties can only be achieved if there is control over the interactions and junctions between particles. From the results, it seems that the rolling process can be used to have this control. Hence, the methodology reported herein can be used to fabricate any type of nanoparticle-based thin films. It can also be extended to other studies in order to have a more comprehensive understanding of advanced materials.

REFERENCES

REFERENCES

[1]   Ozkan, T., M. Naraghi, and I. Chasiotis, *Mechanical properties of vapor grown carbon nanofibers.* Carbon, 2010. **48**(1): p. 239-244.

[2]   Al-Saleh, M.H. and U. Sundararaj, *A review of vapor grown carbon nanofiber/polymer conductive composites.* Carbon, 2009. **47**(1): p. 2-22.

[3]   Zhao, Z.F., J.H. Gou, and A. Khan, *Processing and Structure of Carbon Nanofiber Paper.* Journal of Nanomaterials, 2009. 10.1155/2009/325769.

[4]   Wang, Z., Z. Liang, B. Wang, C. Zhang, and L. Kramer, *Processing and property investigation of single-walled carbon nanotube (SWNT) buckypaper/epoxy resin matrix nanocomposites.* Composites Part A: Applied Science and Manufacturing, 2004. **35**(10): p. 1225-1232.

[5]   Thess, A., R. Lee, P. Nikolaev, H. Dai, P. Petit, J. Robert, C. Xu, Y.H. Lee, S.G. Kim, A.G. Rinzler, D.T. Colbert, G.E. Scuseria, D. Tománek, J.E. Fischer, and R.E. Smalley, *Crystalline Ropes of Metallic Carbon Nanotubes.* Science, 1996. **273**(5274): p. 483-487.

[6]   Rinzler, A.G., J. Liu, H. Dai, P. Nikolaev, C.B. Huffman, F.J. Rodriguez-Macias, P.J. Boul, A.H. Lu, D. Heymann, D.T. Colbert, R.S. Lee, J.E. Fischer, A.M. Rao, P.C. Eklund, and R.E. Smalley, *Large-scale purification of single-wall carbon nanotubes: process, product, and characterization.* Applied Physics A (Materials Science Processing), 1998. **67**(1): p. 29-37.

[7]   Sreekumar, T.V., T. Liu, S. Kumar, L.M. Ericson, R.H. Hauge, and R.E. Smalley, *Single-Wall Carbon Nanotube Films.* Chemistry of Materials, 2002. **15**(1): p. 175-178.

[8]   Berhan, L., Y.B. Yi, A.M. Sastry, E. Munoz, M. Selvidge, and R. Baughman, *Mechanical properties of nanotube sheets: Alterations in joint morphology and achievable moduli in manufacturable materials.* Journal of Applied Physics, 2004. **95**(8): p. 4335-4345.

[9]   Wang, S., Z. Liang, B. Wang, and C. Zhang, *High-strength and multifunctional macroscopic fabric of single-walled carbon nanotubes.* Advanced Materials, 2007. **19**(9): p. 1257-+.

[10]   Malik, S., H. Rosner, F. Hennrich, A. Bottcher, M.M. Kappes, T. Beck, and M. Auhorn, *Failure mechanism of free standing single-walled carbon nanotube thin films under tensile load.* Physical Chemistry Chemical Physics, 2004. **6**(13): p. 3540-3544.

[11]   Nirmalraj, P.N., P.E. Lyons, S. De, J.N. Coleman, and J.J. Boland, *Electrical Connectivity in Single-Walled Carbon Nanotube Networks.* Nano Letters, 2009. **9**(11): p. 3890-3895.

[12]   Ding, W. and et al., *Highly oriented carbon nanotube papers made of aligned carbon nanotubes.* Nanotechnology, 2008. **19**(7): p. 075609.

[13]   Tawfick, S., K. O'Brien, and A.J. Hart, *Flexible High-Conductivity Carbon-Nanotube Interconnects Made by Rolling and Printing.* Small, 2009. **5**(21): p. 2467-2473.

[14]   Oberlin, A., M. Endo, and T. Koyama, *Filamentous growth of carbon through benzene decomposition.* Journal of Crystal Growth, 1976. **32**(3): p. 335-349.

[15]   Iijima, S., *Helical microtubules of graphitic carbon.* Nature, 1991. **354**(6348): p. 56-58.

[16]   Iijima, S. and T. Ichihashi, *Single-shell carbon nanotubes of 1-nm diameter.* Nature, 1993. **363**(6430): p. 603-605.

[17]   Bethune, D.S., C.H. Klang, M.S. de Vries, G. Gorman, R. Savoy, J. Vazquez, and R. Beyers, *Cobalt-catalysed growth of carbon nanotubes with single-atomic-layer walls.* Nature, 1993. **363**(6430): p. 605-607.

[18]   Lv, X., F. Du, Y. Ma, Q. Wu, and Y. Chen, *Synthesis of high quality single-walled carbon nanotubes at large scale by electric arc using metal compounds.* Carbon, 2005. **43**(9): p. 2020-2022.

[19]   Journet, C., W.K. Maser, P. Bernier, A. Loiseau, M.L. de la Chapelle, S. Lefrant, P. Deniard, R. Lee, and J.E. Fischer, *Large-scale production of single-walled carbon nanotubes by the electric-arc technique.* Nature, 1997. **388**(6644): p. 756-758.

[20]   Terrones, M., *Science and technology of the Twenty-First Century: Synthesis, properties, and applications of carbon nanotubes*, in *Annual review of materials research, Volume 33, 2003*. 2003, Annual Reviews: Palo Alto, CA, USA. p. 419-501.

[21]   Guo, T., P. Nikolaev, A.G. Rinzler, D. Tomanek, D.T. Colbert, and R.E. Smalley, *Self-Assembly of Tubular Fullerenes.* The Journal of Physical Chemistry, 1995. **99**(27): p. 10694-10697.

[22]   Eklund, P.C., B.K. Pradhan, U.J. Kim, Q. Xiong, J.E. Fischer, A.D. Friedman, B.C. Holloway, K. Jordan, and M.W. Smith, *Large-Scale Production of Single-Walled Carbon Nanotubes Using Ultrafast Pulses from a Free Electron Laser.* Nano Letters, 2002. **2**(6): p. 561-566.

[23]   Bjorn H., M.H., Jirka C., Ursula D., and Siegmar R., *Arc discharge and laser ablation synthesis of singlewalled carbon nanotubes*. 10.1007/1-4020-4574-32006.

[24]   Nikolaev, P., M.J. Bronikowski, K. Bradley, F. Rohmund, D.T. Colbert, K.A. Smith, and R.E. Smalley, *Gas-phase catalytic growth of single-walled carbon nanotubes from carbon monoxide.* Chemical Physics Letters, 1999. **313**(1-2): p. 91-7.

[25]   Hsu, W.K., J.P. Hare, M. Terrones, H.W. Kroto, D.R.M. Walton, and P.J.F. Harris, *Condensed-phase nanotubes.* Nature, 1995. **377**(6551): p. 687-687.

[26]   Geohegan, D.B., H. Schittenhelm, X. Fan, S.J. Pennycook, A.A. Puretzky, M.A. Guillorn, D.A. Blom, and D.C. Joy, *Condensed phase growth of single-wall carbon nanotubes from laser annealed nanoparticulates.* Applied Physics Letters, 2001. **78**(21): p. 3307-3307.

[27]   Sen, R., S. Suzuki, H. Kataura, and Y. Achiba, *Growth of single-walled carbon nanotubes from the condensed phase.* Chemical Physics Letters, 2001. **349**(5–6): p. 383-388.

[28]   Meyyappan, M., D. Lance, C. Alan, and H. David, *Carbon nanotube growth by PECVD: a review.* Plasma Sources Science and Technology, 2003. **12**(2): p. 205.

[29]   Öncel, Ç. and Y. Yürüm, *Carbon Nanotube Synthesis via the Catalytic CVD Method: A Review on the Effect of Reaction Parameters.* Fullerenes, Nanotubes and Carbon Nanostructures, 2006. **14**(1): p. 17-37.

[30]   Cheung, C.L., A. Kurtz, H. Park, and C.M. Lieber, *Diameter-Controlled Synthesis of Carbon Nanotubes.* The Journal of Physical Chemistry B, 2002. **106**(10): p. 2429-2433.

[31]   Deck, C.P. and K. Vecchio, *Growth mechanism of vapor phase CVD-grown multi-walled carbon nanotubes.* Carbon, 2005. **43**(12): p. 2608-2617.

[32]   Dervishi, E., Z. Li, F. Watanabe, V. Saini, A.R. Biris, Y. Xu, and A.S. Biris, *High-aspect ratio and horizontally oriented carbon nanotubes synthesized by RF-cCVD.* Diamond and Related Materials, 2010. **19**(1): p. 67-72.

[33]   Du, C. and N. Pan, *CVD growth of carbon nanotubes directly on nickel substrate.* Materials Letters, 2005. **59**(13): p. 1678-1682.

[34]   Pascault, J.-P., *Thermosetting polymers*. Plastics engineering. 2002, New York: Marcel Dekker. viii, 477 p.

[35]   Zhao, X., Y. Liu, S. Inoue, T. Suzuki, R.O. Jones, and Y. Ando, *Smallest carbon nanotube is 3 A in diameter.* Physical Review Letters, 2004. **92**(12): p. 125502-1-125502-3.

[36]   Reddy, J.N., *An introduction to the finite element method*. 3rd ed. McGraw-Hill series in mechanical engineering. 2006, New York, NY: McGraw-Hill Higher Education. xvi, 766 p.

[37]   Ebbesen, T.W. and P.M. Ajayan, *Large-scale synthesis of carbon nanotubes.* Nature, 1992. **358**(6383): p. 220-222.

[38]   Colbert, D.T., J. Zhang, S.M. Mcclure, P. Nikolaev, Z. Chen, J.H. Hafner, D.W. Owens, P.G. Kotula, C.B. Carter, J.H. Weaver, A.G. Rinzler, and R.E. Smalley, *Growth and Sintering of Fullerene Nanotubes.* Science, 1994. **266**(5188): p. 1218-1222.

[39]   Archer, M.D. and R. Hill, *Clean Electricity from Photovoltaics*. Vol. 1. 2001: World Scientific.

[40]   Bauchspies, W.K., *Everyday practice of science: where intuition and passion meet objectivity and logic*. Choice: Current Reviews for Academic Libraries. Vol. 46. 2009. 2134-2134.

[41]   Kanninen, M.F. and C.H. Popelar, *Advanced Fracture Mechanics*. 1985: Oxford University Press.

[42]   Chiang, I.W., B.E. Brinson, A.Y. Huang, P.A. Willis, M.J. Bronikowski, J.L. Margrave, R.E. Smalley, and R.H. Hauge, *Purification and characterization of single-wall carbon*

nanotubes (SWNTs) obtained from the gas-phase decomposition of CO (HiPco process). Journal of Physical Chemistry B, 2001. **105**(35): p. 8297-301.

[43]   Bandow, S., S. Asaka, Y. Saito, A.M. Rao, L. Grigorian, E. Richter, and P.C. Eklund, *Effect of the growth temperature on the diameter distribution and chirality of single-wall carbon nanotubes.* Physical Review Letters, 1998. **80**(17): p. 3779-3782.

[44]   Sen, R., Y. Ohtsuka, T. Ishigaki, D. Kasuya, S. Suzuki, H. Kataura, and Y. Achiba, *Time period for the growth of single-wall carbon nanotubes in the laser ablation process: evidence from gas dynamic studies and time resolved imaging.* Chemical Physics Letters, 2000. **332**(5-6): p. 467-473.

[45]   Kataura, H., Y. Kumazawa, Y. Maniwa, Y. Ohtsuka, R. Sen, S. Suzuki, and Y. Achiba, *Diameter control of single-walled carbon nanotubes.* Carbon, 2000. **38**(11-12): p. 1691-1697.

[46]   Brown, D., *The lost symbol.* 1st ed. 2010, New York: Doubleday. 513 p.

[47]   Walker, P.L., J.F. Rakszawski, and G.R. Imperial, *Carbon Formation from Carbon Monoxide-Hydrogen Mixtures over Iron Catalysts.I. Properties of Carbon Formed.* The Journal of Physical Chemistry, 1959. **63**(2): p. 133-140.

[48]   Tamin, M.N.N., *Damage and fracture of composite materials and structures.* 2011, New York: Springer.

[49]   Gillespie, J.W., *Delamination growth in composite materialsJohn* NASA CR-176416. 1985: Center for Composite Materials, College of Engineering, University of Delaware

National Aeronautics and Space Administration (NASA). 1-24.

[50]   Li, Y.-H., C. Xu, B. Wei, X. Zhang, M. Zheng, D. Wu, and P.M. Ajayan, *Self-organized Ribbons of Aligned Carbon Nanotubes.* Chemistry of Materials, 2002. **14**(2): p. 483-485.

[51]   Hernadi, K., A. Fonseca, J.B. Nagy, D. Bernaerts, and A.A. Lucas, *Fe-catalyzed carbon nanotube formation.* Carbon, 1996. **34**(10): p. 1249-1257.

[52]   Minjae, J., E. Kwang Yong, L. Jae-Kap, B. Young-Joon, L. Kwang-Ryeol, and P. Jong Wan. *Growth of carbon nanotubes by chemical vapor deposition.* 2001. Switzerland: Elsevier.

[53]   Dal, H.J., A.G. Rinzler, P. Nikolaev, A. Thess, D.T. Colbert, and R.E. Smalley, *Single-wall nanotubes produced by metal-catalyzed disproportionation of carbon monoxide.* Chemical Physics Letters, 1996. **260**(3-4): p. 471-475.

[54]   Cheng, H.M., F. Li, X. Sun, S.D.M. Brown, M.A. Pimenta, A. Marucci, G. Dresselhaus, and M.S. Dresselhaus, *Bulk morphology and diameter distribution of single-walled carbon nanotubes synthesized by catalytic decomposition of hydrocarbons.* Chemical Physics Letters, 1998. **289**(5-6): p. 602-610.

[55] Satishkumar, B.C., A. Govindaraj, R. Sen, and C.N.R. Rao, *Single-walled nanotubes by the pyrolysis of acetylene-organometallic mixtures.* Chemical Physics Letters, 1998. **293**(1-2): p. 47-52.

[56] Hafner, J.H., M.J. Bronikowski, B.R. Azamian, P. Nikolaev, A.G. Rinzler, D.T. Colbert, K.A. Smith, and R.E. Smalley, *Catalytic growth of single-wall carbon nanotubes from metal particles.* Chemical Physics Letters, 1998. **296**(1-2): p. 195-202.

[57] Ago, H., S. Ohshima, K. Uchida, and M. Yumura, *Gas-Phase Synthesis of Single-wall Carbon Nanotubes from Colloidal Solution of Metal Nanoparticles.* The Journal of Physical Chemistry B, 2001. **105**(43): p. 10453-10456.

[58] Ago, H., T. Komatsu, S. Ohshima, Y. Kuriki, and M. Yumura, *Dispersion of metal nanoparticles for aligned carbon nanotube arrays.* Applied Physics Letters, 2000. **77**(1): p. 79-81.

[59] Odom, T.W., H. Jin-Lin, P. Kim, and C.M. Lieber, *Atomic structure and electronic properties of single-walled carbon nanotubes.* Nature, 1998. **391**(6662): p. 62-4.

[60] Wildoer, J.W.G., L.C. Venema, A.G. Rinzler, R.E. Smalley, and C. Dekker, *Electronic structure of atomically resolved carbon nanotubes.* Nature, 1998. **391**(6662): p. 59-62.

[61] Charlier, J.C., *Defects in Carbon Nanotubes.* Accounts of Chemical Research, 2002. **35**(12): p. 1063-1069.

[62] Thostenson, E.T., R. Zhifeng, and C. Tsu-Wei, *Advances in the science and technology of carbon nanotubes and their composites: a review.* Composites Science and Technology, 2001. **61**(13): p. 1899-912.

[63] Saito, R., M. Fujita, G. Dresselhaus, and M.S. Dresselhaus, *Electronic structure of graphene tubules based on C_{60}.* Physical Review B, 1992. **46**(3): p. 1804-1811.

[64] Saito, R., M. Fujita, G. Dresselhaus, and M.S. Dresselhaus, *Electronic structure of chiral graphene tubules.* Applied Physics Letters, 1992. **60**(18): p. 2204-2206.

[65] Dresselhaus, M.S., G. Dresselhaus, J.C. Charlier, and E. Hernandez, *Electronic, thermal and mechanical properties of carbon nanotubes.* Philosophical Transactions of the Royal Society London, Series A (Mathematical, Physical and Engineering Sciences), 2004. **362**(1823): p. 2065-98.

[66] Vaccarini, L., C. Goze, L. Henrard, E. Hernández, P. Bernier, and A. Rubio, *Mechanical and electronic properties of carbon and boron–nitride nanotubes.* Carbon, 2000. **38**(11–12): p. 1681-1690.

[67] Yakobson, B.I., C.J. Brabec, and J. Bernholc, *Nanomechanics of Carbon Tubes: Instabilities beyond Linear Response.* Physical Review Letters, 1996. **76**(14): p. 2511.

[68] Troya, D., S.L. Mielke, and G.C. Schatz, *Carbon nanotube fracture-differences between quantum mechanical mechanisms and those of empirical potentials.* Chemical Physics Letters, 2003. **382**(1-2): p. 133-41.

[69] Xin Haoa, H.Q., a, and Yao Xiaohu, *Buckling of defective single-walled and double-walled carbon nanotubes under axial compression by molecular dynamics simulation* Composites Science and Technology, 2008. **68**(7-8): p. 1809-1814.

[70] Lu, Q. and B. Bhattacharya, *The role of atomistic simulations in probing the small-scale aspects of fracture--a case study on a single-walled carbon nanotube.* Engineering Fracture Mechanics, 2005. **72**(13): p. 2037-2071.

[71] Guzman, M.E., *Enhancement of mechanical properties of a potting compound by addition of functionalized single-walled and multi-walled carbon nanotubes*, in *Mechanical Engineering*. 2010, Wichita State University: Wichita. p. 81.

[72] Nardelli, M.B., B.I. Yakobson, and J. Bernholc, *Brittle and ductile behavior in carbon nanotubes.* Physical Review Letters, 1998. **81**(21): p. 4656-4659.

[73] Hughes, T.V. and C.R. Chambers, *Manufacture of Carbon Filaments*, U.S. Patents, Editor. 1889.

[74] Koyama, T. and M. Endo, *Structure and growth processes of vapor-grown carbon fibers*. 1983, NASA. p. 23.

[75] Tibbetts, G.G., M.L. Lake, K.L. Strong, and B.P. Rice, *A review of the fabrication and properties of vapor-grown carbon nanofiber/polymer composites.* Composites Science and Technology, 2007. **67**(7–8): p. 1709-1718.

[76] Endo, M., *Grow Carbon-Fibers in the Vapor-Phase.* Chemtech, 1988. **18**(9): p. 568-576.

[77] Rodriguez, N.M., A. Chambers, and R.T.K. Baker, *Catalytic Engineering of Carbon Nanostructures.* Langmuir, 1995. **11**(10): p. 3862-3866.

[78] Krishnan, A., E. Dujardin, M.M.J. Treacy, J. Hugdahl, S. Lynum, and T.W. Ebbesen, *Graphitic cones and the nucleation of curved carbon surfaces.* Nature, 1997. **388**(6641): p. 451-454.

[79] Endo, M., Y.A. Kim, T. Hayashi, Y. Fukai, K. Oshida, M. Terrones, T. Yanagisawa, S. Higaki, and M.S. Dresselhaus, *Structural characterization of cup-stacked-type nanofibers with an entirely hollow core.* Applied Physics Letters, 2002. **80**(7): p. 1267-1269.

[80] Merkulov, V.I., D.H. Lowndes, Y.Y. Wei, G. Eres, and E. Voelkl, *Patterned growth of individual and multiple vertically aligned carbon nanofibers.* Applied Physics Letters, 2000. **76**(24): p. 3555-3557.

[81] Uchida, T., D. Anderson, M. Minus, and S. Kumar, *Morphology and modulus of vapor grown carbon nano fibers.* Journal of Materials Science, 2006. **41**(18): p. 5851-5856.

[82] Miyagawa, H., M.J. Rich, and L.T. Drzal, *Thermo-physical properties of epoxy nanocomposites reinforced by carbon nanotubes and vapor grown carbon fibers.* Thermochimica Acta, 2006. **442**(1-2): p. 67-73.

[83]   Jimenez, G.A. and S.C. Jana, *Electrically conductive polymer nanocomposites of polymethylmethacrylate and carbon nanofibers prepared by chaotic mixing.* Composites Part A: Applied Science and Manufacturing, 2007. **38**(3): p. 983-993.

[84]   Endo, M., Y.A. Kim, T. Hayashi, K. Nishimura, T. Matusita, K. Miyashita, and M.S. Dresselhaus, *Vapor-grown carbon fibers (VGCFs): Basic properties and their battery applications.* Carbon, 2001. **39**(9): p. 1287-1297.

[85]   Prolongo, S.G., M. Campo, M.R. Gude, R. Chaos-Moran, and A. Urena, *Thermo-physical characterisation of epoxy resin reinforced by amino-functionalized carbon nanofibers.* Composites Science and Technology, 2009. **69**(3-4): p. 349-357.

[86]   Buffa, F., G.A. Abraham, B.P. Grady, and D. Resasco, *Effect of nanotube functionalization on the properties of single-walled carbon nanotube/polyurethane composites.* Journal of Polymer Science Part B: Polymer Physics, 2007. **45**(4): p. 490-501.

[87]   Lakshminarayanan, P.V., H. Toghiani, and C.U. Pittman Jr, *Nitric acid oxidation of vapor grown carbon nanofibers.* Carbon, 2004. **42**(12-13): p. 2433-2442.

[88]   Dongil, A.B., B. Bachiller-Baeza, A. Guerrero-Ruiz, I. Rodríguez-Ramos, A. Martínez-Alonso, and J.M.D. Tascón, *Surface chemical modifications induced on high surface area graphite and carbon nanofibers using different oxidation and functionalization treatments.* Journal of Colloid and Interface Science, 2011. **355**(1): p. 179-189.

[89]   Chen, C., B. Liang, D. Lu, A. Ogino, X. Wang, and M. Nagatsu, *Amino group introduction onto multiwall carbon nanotubes by NH3/Ar plasma treatment.* Carbon, 2010. **48**(4): p. 939-948.

[90]   Georgakilas, V., K. Kordatos, M. Prato, D.M. Guldi, M. Holzinger, and A. Hirsch, *Organic Functionalization of Carbon Nanotubes.* Journal of the American Chemical Society, 2002. **124**(5): p. 760-761.

[91]   Miller, S.G., J.L. Bauer, M.J. Maryanski, P.J. Heimann, J.P. Barlow, J.-M. Gosau, and R.E. Allred, *Characterization of epoxy functionalized graphite nanoparticles and the physical properties of epoxy matrix nanocomposites.* Composites Science and Technology, 2010. **70**(7): p. 1120-1125.

[92]   Spitalsky, Z., D. Tasis, K. Papagelis, and C. Galiotis, *Carbon nanotube-polymer composites: Chemistry, processing, mechanical and electrical properties.* Progress in Polymer Science, 2010. **35**(3): p. 357-401.

[93]   Bose, S., R.A. Khare, and P. Moldenaers, *Assessing the strengths and weaknesses of various types of pre-treatments of carbon nanotubes on the properties of polymer/carbon nanotubes composites: A critical review.* Polymer, 2010. **51**(5): p. 975-993.

[94]   Lachman, N. and H. Daniel Wagner, *Correlation between interfacial molecular structure and mechanics in CNT/epoxy nano-composites.* Composites Part A: Applied Science and Manufacturing, 2010. **41**(9): p. 1093-1098.

[95]   Seyhan, A.T., Z. Sun, J. Deitzel, M. Tanoglu, and D. Heider, *Cure kinetics of vapor grown carbon nanofiber (VGCNF) modified epoxy resin suspensions and fracture toughness of their resulting nanocomposites.* Materials Chemistry and Physics, 2009. **118**(1): p. 234-242.

[96]   Prolongo, S.G., M. Burón, M.R. Gude, R. Chaos-Morán, M. Campo, and A. Ureña, *Effects of dispersion techniques of carbon nanofibers on the thermo-physical properties of epoxy nanocomposites.* Composites Science and Technology, 2008. **68**(13): p. 2722-2730.

[97]   Gong, X., J. Liu, S. Baskaran, R.D. Voise, and J.S. Young, *Surfactant-Assisted Processing of Carbon Nanotube/Polymer Composites.* Chemistry of Materials, 2000. **12**(4): p. 1049-1052.

[98]   Geng, Y., M.Y. Liu, J. Li, X.M. Shi, and J.K. Kim, *Effects of surfactant treatment on mechanical and electrical properties of CNT/epoxy nanocomposites.* Composites Part A: Applied Science and Manufacturing, 2008. **39**(12): p. 1876-1883.

[99]   Vaisman, L., H.D. Wagner, and G. Marom, *The role of surfactants in dispersion of carbon nanotubes.* Advances in Colloid and Interface Science, 2006. **128–130**(0): p. 37-46.

[100]   Shelimov, K.B., R.O. Esenaliev, A.G. Rinzler, C.B. Huffman, and R.E. Smalley, *Purification of single-wall carbon nanotubes by ultrasonically assisted filtration.* Chemical Physics Letters, 1998. **282**(5-6): p. 429-434.

[101]   Shimamoto, D., K. Fujisawa, H. Muramatsu, T. Hayashi, Y.A. Kim, T. Yanagisawa, M. Endo, and M.S. Dresselhaus, *A simple route to short cup-stacked carbon nanotubes by sonication.* Carbon, 2010. **48**(12): p. 3643-3647.

[102]   Na, X., J. Qingjie, Z. Chongguang, W. Chenglong, and L. Yuanyuan, *Study on dispersion and electrical property of multi-walled carbon nanotubes/low-density polyethylene nanocomposites.* Materials & Design. **31**(4): p. 1676-1683.

[103]   Gojny, F.H., M.H.G. Wichmann, U. Köpke, B. Fiedler, and K. Schulte, *Carbon nanotube-reinforced epoxy-composites: enhanced stiffness and fracture toughness at low nanotube content.* Composites Science and Technology, 2004. **64**(15): p. 2363-2371.

[104]   Prolongo, S.G., M.R. Gude, Ure, and A. a, *Rheological Behaviour of Nanoreinforced Epoxy Adhesives of Low Electrical Resistivity for Joining Carbon Fiber/Epoxy Laminates.* Journal of Adhesion Science and Technology. **24**(6): p. 1097-1112.

[105]   Tsu-Wei, C. and E.T. Thostenson, *Processing-structure-multi-functional property relationship in carbon nanotube/epoxy composites.* Carbon, 2006. **44**(14): p. 3022-9.

[106]   Khalid Lafdi, W.F., Matthew Matzek, and Emel Yildiz, *Effect of Carbon Nanofiber-Matrix Adhesion on Polymeric Nanocomposite Properties—Part II.* Journal of nanomaterials, 2007. **2008**.

[107]   Bortz, D.R., C. Merino, and I. Martin-Gullon, *Carbon nanofibers enhance the fracture toughness and fatigue performance of a structural epoxy system.* Composites Science and Technology, 2011. **71**(1): p. 31-38.

[108]   Guzman, M.E., A.J. Rodriguez, B. Minaie, and M. Violette, *Processing and properties of syntactic foams reinforced with carbon nanotubes.* Journal of Applied Polymer Science, 2012. **124**(3): p. 2383-2394.

[109]   Joong Tark, H., J. Hee Jin, and L. Geon-Woong. *Buckypaper from thin multiwalled carbon nanotubes.* in *Carbon Nanotubes and Associated Devices, 10 Aug. 2008.* 2008. USA: SPIE - The International Society for Optical Engineering.

[110]   Gou, J., S. Braint, H. Gu, and G. Song, *Damping Augmentation of Nanocomposites Using Carbon Nanofiber Paper.* Journal of Nanomaterials, 2006. **2006**.

[111]   Wei, B.Q., R. Vajtai, Y. Jung, J. Ward, R. Zhang, G. Ramanath, and P.M. Ajayan, *Assembly of Highly Organized Carbon Nanotube Architectures by Chemical Vapor Deposition.* Chemistry of Materials, 2003. **15**(8): p. 1598-1606.

[112]   Wei, B.Q., R. Vajtai, Y. Jung, J. Ward, R. Zhang, G. Ramanath, and P.M. Ajayan, *Organized assembly of carbon nanotubes - Cunning refinements help to customize the architecture of nanotube structures.* Nature, 2002. **416**(6880): p. 495-496.

[113]   Pint, C.L., Y.-Q. Xu, M. Pasquali, and R.H. Hauge, *Formation of highly dense aligned ribbons and transparent films of single-walled carbon nanotubes directly from carpets.* ACS Nano, 2008. **2**(Compendex): p. 1871-1878.

[114]   Kim, S.-K. and H. Lee, *Fabrication of patterned single-walled carbon nanotube films using electrophoretic deposition.* Ultramicroscopy, 2008. **108**(10): p. 1005-1008.

[115]   Kim, S.-K., H. Lee, H. Tanaka, and P.S. Weiss, *Vertical Alignment of Single-Walled Carbon Nanotube Films Formed by Electrophoretic Deposition.* Langmuir, 2008. **24**(22): p. 12936-12942.

[116]   Hu, L., D.S. Hecht, and G. Grüner, *Percolation in Transparent and Conducting Carbon Nanotube Networks.* Nano Letters, 2004. **4**(12): p. 2513-2517.

[117]   Ma, Y., B. Wang, Y. Wu, Y. Huang, and Y. Chen, *The production of horizontally aligned single-walled carbon nanotubes.* Carbon, 2011. **49**(13): p. 4098-4110.

[118]   Kim, Y., N. Minami, W.H. Zhu, S. Kazaoui, R. Azumi, and M. Matsumoto, *Langmuir-Blodgett films of single-wall carbon nanotubes: Layer-by-layer deposition and in-plane orientation of tubes.* Japanese Journal of Applied Physics Part 1-Regular Papers Short Notes & Review Papers, 2003. **42**(12): p. 7629-7634.

[119]   Giancane, G., A. Ruland, V. Sgobba, D. Manno, A. Serra, G.M. Farinola, O.H. Omar, D.M. Guldi, and L. Valli, *Aligning Single-Walled Carbon Nanotubes By Means Of Langmuir-Blodgett Film Deposition: Optical, Morphological, and Photo-electrochemical Studies.* Advanced Functional Materials, 2010. **20**(15): p. 2481-2488.

[120]   Lee, S.W., B.-S. Kim, S. Chen, Y. Shao-Horn, and P.T. Hammond, *Layer-by-Layer Assembly of All Carbon Nanotube Ultrathin Films for Electrochemical Applications.* Journal of the American Chemical Society, 2008. **131**(2): p. 671-679.

[121] Liu, Z., Z. Shen, T. Zhu, S. Hou, L. Ying, Z. Shi, and Z. Gu, *Organizing Single-Walled Carbon Nanotubes on Gold Using a Wet Chemical Self-Assembling Technique.* Langmuir, 2000. **16**(8): p. 3569-3573.

[122] Liu, J., A.G. Rinzler, H. Dai, J.H. Hafner, R.K. Bradley, P.J. Boul, A. Lu, T. Iverson, K. Shelimov, C.B. Huffman, F. Rodriguez-Macias, Y.-S. Shon, T.R. Lee, D.T. Colbert, and R.E. Smalley, *Fullerene Pipes.* Science, 1998. **280**(5367): p. 1253-1256.

[123] Muramatsu, H., T. Hayashi, Y.A. Kim, D. Shimamoto, Y.J. Kim, K. Tantrakarn, M. Endo, M. Terrones, and M.S. Dresselhaus, *Pore structure and oxidation stability of double-walled carbon nanotube-derived bucky paper.* Chemical Physics Letters, 2005. **414**(4–6): p. 444-448.

[124] Li, Z., J. Xu, J.P. O'Byrne, L. Chen, K. Wang, M.A. Morris, and J.D. Holmes, *Freestanding bucky paper with high strength from multi-wall carbon nanotubes.* Materials Chemistry and Physics. 10.1016/j.matchemphys.2012.05.080(0).

[125] Gou, J., S. Sumerlin, H.C. Gu, and G. Song. *Damping enhancement of hybrid nanocomposites embedded with engineered carbon nanopaper*. in *2006 ASME International Mechanical Engineering Congress and Exposition, IMECE2006, November 5, 2006 - November 10, 2006*. 2006. Chicago, IL, United states: American Society of Mechanical Engineers.

[126] Bradford, P.D., X. Wang, H. Zhao, J.-P. Maria, Q. Jia, and Y.T. Zhu, *A novel approach to fabricate high volume fraction nanocomposites with long aligned carbon nanotubes.* Composites Science and Technology, 2010. **70**(13): p. 1980-1985.

[127] Liu, W., X. Zhang, G. Xu, P.D. Bradford, X. Wang, H. Zhao, Y. Zhang, Q. Jia, F.-G. Yuan, Q. Li, Y. Qiu, and Y. Zhu, *Producing superior composites by winding carbon nanotubes onto a mandrel under a poly(vinyl alcohol) spray.* Carbon, 2011. **49**(14): p. 4786-4791.

[128] Applied Science, I. *Pyrograpf III*. 2012 Dec. 13, 2012]; Available from: http://apsci.com/?page_id=19.

[129] Rodriguez, A.J., M.E. Guzman, C.-S. Lim, and B. Minaie, *Synthesis of multiscale reinforcement fabric by electrophoretic deposition of amine-functionalized carbon nanofibers onto carbon fiber layers.* Carbon, 2010. **48**(11): p. 3256-3259.

[130] Instruments, L.S. *TST350*. 2010 Jan. 12, 2012]; Tensile Stage]. Available from: http://www.linkam.co.uk/storage/product-brochures/Tensile_System_TST350_v1.4.pdf.

[131] Keithley, *Model 2000 Multimeter*, Keithley, Editor. 2003.

[132] Zhu, J., H. Peng, F. Rodriguez-Macias, J.L. Margrave, V.N. Khabashesku, A.M. Imam, K. Lozano, and E.V. Barrera, *Reinforcing Epoxy Polymer Composites Through Covalent Integration of Functionalized Nanotubes.* Advanced Functional Materials, 2004. **14**(7): p. 643-648.

[133] Wang, Y., Z. Iqbal, and S. Mitra, *Rapidly Functionalized, Water-Dispersed Carbon Nanotubes at High Concentration.* J. Am. Chem. Soc., 2006. **128**(1): p. 95-99.

[134] Figueiredo, J.L., M.F.R. Pereira, M.M.A. Freitas, and J.J.M. Órfão, *Modification of the surface chemistry of activated carbons.* Carbon, 1999. **37**(9): p. 1379-1389.

[135] Lim, C.S., M. Guzman, J. Schaefer, and B. Minaie, *Fabrication and properties of dense thin films containing functionalized carbon nanofibers.* Thin Solid Films, 2013. **534**(0): p. 111-115.

[136] Arunan, E., G.R. Desiraju, R.A. Klein, J. Sadlej, S. Scheiner, I. Alkorta, D.C. Clary, R.H. Crabtree, J.J. Dannenberg, P. Hobza, H.G. Kjaergaard, A.C. Legon, B. Mennucci, and D.J. Nesbitt, *Definition of the hydrogen bond (IUPAC Recommendations 2011).* Pure and Applied Chemistry, 2011. **83**(8): p. 1637-1641.

[137] Han, J.T., S.Y. Kim, J.S. Woo, H.J. Jeong, W. Oh, and G.-W. Lee, *Hydrogen-Bond-Driven Assembly of Thin Multiwalled Carbon Nanotubes.* The Journal of Physical Chemistry C, 2008. **112**(41): p. 15961-15965.

[138] Kukovecz, A., C. Kramberger, M. Holzinger, H. Kuzmany, J. Schalko, M. Mannsberger, and A. Hirsch, *On the Stacking Behavior of Functionalized Single-Wall Carbon Nanotubes.* The Journal of Physical Chemistry B, 2002. **106**(25): p. 6374-6380.

[139] Sebastián, D., I. Suelves, R. Moliner, and M.J. Lázaro, *The effect of the functionalization of carbon nanofibers on their electronic conductivity.* Carbon, 2010. **48**(15): p. 4421-4431.

[140] Celzard, A., J.F. Marêché, F. Payot, and G. Furdin, *Electrical conductivity of carbonaceous powders.* Carbon, 2002. **40**(15): p. 2801-2815.

[141] Euler, K.-J., *The conductivity of compressed powders. A review.* Journal of Power Sources, 1978. **3**(2): p. 117-136.

[142] Pantea, D., H. Darmstadt, S. Kaliaguine, L. Sümmchen, and C. Roy, *Electrical conductivity of thermal carbon blacks: Influence of surface chemistry.* Carbon, 2001. **39**(8): p. 1147-1158.

[143] Yang, K., J. He, Z. Su, J.B. Reppert, M.J. Skove, T.M. Tritt, and A.M. Rao, *Inter-tube bonding, graphene formation and anisotropic transport properties in spark plasma sintered multi-wall carbon nanotube arrays.* Carbon, 2010. **48**(3): p. 756-762.

[144] Cheng, Q., J. Bao, J. Park, Z. Liang, C. Zhang, and B. Wang, *High Mechanical Performance Composite Conductor: Multi-Walled Carbon Nanotube Sheet/Bismaleimide Nanocomposites.* Advanced Functional Materials, 2009. **19**(20): p. 3219-3225.